1985

Verification of a Numerical Ocean Model of the Arabian Sea

Ray C. Simmons

Mark E. Luther
Florida State University, mluther@usf.edu

JOURNAL OF GEOPHYSICAL RESEARCH, VOL. 93, NO. C12, PAGES 15,437–15,453, DECEMBER 15, 1988

Verification of a Numerical Ocean Model of the Arabian Sea

RAY C. SIMMONS,[1] MARK E. LUTHER, JAMES J. O'BRIEN, AND DAVID M. LEGLER

Mesoscale Air-Sea Interaction Group, Florida State University, Tallahassee

A case study evaluating the predictive capability of an upper layer circulation model of the northwest Indian Ocean is presented. The model is a nonlinear, reduced gravity model incorporating realistic boundary geometry and is forced by observed winds. Model results for the fall of 1985 are compared with and evaluated against U.S. Navy bathythermograph and NOAA satellite data collected during August–November 1985. An assessment is made of the model's ability to simulate correctly the circulation structure. Ship wind observations are converted to wind stress for model forcing by a procedure developed by Legler and Navon (1988). The model is only moderately successful in reproducing the structure of the large, rather homogeneous pool of water located off the Arabian Peninsula in September. However, the model behaves remarkably well in the dynamically active region around Socotra. Major fronts and eddies frequently observed in the region during the transition period between the southwest and the northeast monsoon appear in the 1985 model results and compare well, both temporally and spatially, with the observational data. Thus given accurate wind information, the model appears highly effective in dynamically active regions and demonstrates potential as a useful prognostic tool for evaluation of the Arabian Sea when real time winds become available.

INTRODUCTION

Forced by the semiannually reversing northeast and southwest monsoonal winds, circulation patterns of the northwest Indian Ocean, the Arabian Sea, have intrigued oceanographers for many years. Of particular interest is the Somali Current, unique to the region, with its reversing flow and dynamically active circulation structure, characterized by a very complex system of eddies and fronts.

During the northern winter the northeast monsoon drives northeasterly winds and a corresponding southward boundary current along the Somali coast. During the transition from winter into spring, the northeast monsoon relaxes, and the coastal current reverses along Kenya and southern Somalia. By mid-April, the southern hemisphere trade winds extend well to the northwest, and a northward surface current flows to the equator, where it turns offshore and recirculates to the south forming a southern gyre. By May the winds reverse all along the Somali coast and form a jetlike atmospheric structure [*Findlater*, 1971], analogous to an oceanic western boundary current, which is confined in the west by the highlands of Kenya and Ethiopia and remains over land at very low latitudes. In June the core of this atmospheric jet crosses the coast at about 8°N and becomes very strong. A second oceanic gyre forms in the Somali Current between 4°N and 10°N to which *Findlay* [1866] attached the name "great whirl." This two-gyre system intensifies throughout June and is well established by mid to late July, when the winds again begin to weaken and the two gyres coalesce and begin a slow migration to the north. Extensive observations [e.g., *Bruce*, 1973, 1979, 1983; *Brown et al.*, 1980; *Evans and Brown*, 1981; *Swallow and Fieux*, 1982; *Schott*, 1983; *Swallow et al.*, 1983] have shown this dynamic structure along the African coast to be relatively consistent from year to year during the southwest monsoon.

In October the winds begin to reverse, indicating the onset of the northeast monsoon, and the southward Somali current again develops. Prior to a complete wind shift, a complicated dynamic circulation structure develops around Socotra and along the Arabian peninsula. To date, little attention has been focused on this fall circulation structure; however, *Cagle and Whritner* [1981] used satellite infrared imagery to observe and describe a number of the complicated dynamic features of the region. They concluded from their study that the various eddies and wedges found in the northern Arabian Sea during the breakdown of the southwest monsoon are a response to wind forcing and topographic features associated with the coastal geometry. The study presented here investigates these fall dynamic features, with particular emphasis centered on the northwest Arabian Sea, north of Socotra, during September–November 1985.

Cox [1970] was the first to attempt a large-scale numerical model of the Indian Ocean, using an early version of the Bryan-Cox or Geophysical Fluid Dynamics Laboratory (GFDL) model. The model, driven by idealizations of observed wind stress and temperature-salinity data and integrated over 2 centuries, reproduced the reversal of the Somali Current and most of the other large-scale circulation features of the region, but limited resolution prohibited simulation of many small-scale features. This was an important result, however, as it was inferred from this investigation that the rapid spin-up of the Somali Current at the beginning of the southwest monsoon was due to local winds, as compared with *Lighthill*'s [1969] result which hypothesized that the Somali Current is remotely forced by westward propogating equatorial Rossby waves generated by winds within the Indian Ocean interior. *Anderson and Rowlands* [1976] investigated this problem and were able to show analytically that local forcing is important initially but that remote forcing effects become important over time. *Cox* [1976] was able to confirm this with his model but also showed that friction and nonlinear effects modify their result and that nonlinear horizontal shearing instabilities are able to produce eddies similar to those observed in the Somali Current system.

[1]Now at NAVWEST Ocean Center, Pearl Harbor, Hawaii.

Paper number 88JC03477.
0148-0227/88/88JC-03477$05.00

The northward migration of the great whirl was investigated by *Hurlburt and Thompson* [1976] using a two-layer numerical model in which they showed that nonlinear eddies, formed at the equator by an impulsively applied wind stress, could indeed move northward along the coast as a result of advective effects. *Cox* [1979] extended this investigation by incorporating effects of boundary orientation on the northward advection of the eddies and determined that migration is dependent upon boundary slope and is arrested for slopes of greater than 45°. The net result of these studies was *Cox*'s [1981] conclusion that eddy movement is dependent upon advection of vorticity, vortex stretching, the beta effect, and the wind stress curl.

Further numerical studies have been conducted by *Anderson and Moore* [1979], who took the Somali Current to be a free inertial cross-equatorial jet remotely forced by the southern hemisphere trade winds and found reasonable separation latitudes for the southern gyre of the Somali Current. *Lin and Hurlburt* [1981] used a reduced gravity model with an impulsively applied wind, parallel to the coast and constant alongshore, to reproduce two equatorial eddies that subsequently migrated northward. *Anderson* [1981], again with a reduced gravity model, showed that the southernmost gyre could be generated by the northwest penetration of the southern hemisphere trade winds at the onset of the southwest monsoon, while the northern gyre results from the departure from the Somali coast around 9°N of Findlater's low-level wind jet. Observations, described by *Schott and Quadfasel* [1982], further indicate that the local curl of the wind stress in the development of the low-level jet also plays a significant role in formation of the great whirl.

The above described large-scale features are repeatable phenomena in many numerical studies. Numerous small-scale features (eddies, wedges, and fronts) are less repeatable in models and appear to be highly dependent upon the structure of the wind forcing. A number of observations have described these features along the African coast during the southwest monsoon [*Bruce*, 1973, 1979, 1983; *Brown et al.*, 1980]. Far less attention has been devoted to the eddies and fronts found around and to the north of Socotra as the northeastward Somali Current breaks down during the transition into the southwestward Somali Current during the northern fall.

Luther and O'Brien [1985] developed the model used in this study and forced it with climatological winds to reproduce most of the observed features of the Somali Current system. The presence of a large, time-varying region of wind stress curl within and just offshore of the boundary region, as well as the inclusion of the entire seasonal cycle, was found to be critical for the accurate simulation of observed circulation patterns. Further study by *Luther et al.* [1985] used the same model, driven by the monthly mean winds from the First GARP Global Experiment and monthly mean climatological winds, and again reproduced the observed features of the region. An assessment was made of the effects of various forcing mechanisms (spatial and temporal inhomogeneity of the winds, negative vorticity input by the wind stress curl, and differential Ekman pumping) on the generation and decay of the two-gyre system.

In the present study, ship-observed winds for 1985 are used to force the model and generate the resultant dynamic response. Features present north of and around Socotra during the decay of the northeast Somali Current are then analyzed and compared with observations made during the period September–November 1985, for which U.S. Navy expendable bathythermograph (XBT) and NOAA advanced very high resolution radiometer (AVHRR) satellite images were collected and analyzed for the region.

In subsequent sections a brief description of the model is followed by a description of the available wind and oceanographic data, and finally an evaluation and assessment of the model's ability to effectively predict Arabian Sea dynamics, given reasonably accurate actual winds, is made based on the available XBT and satellite data.

THE MODEL

The nonlinear reduced gravity transport equations are used to model the upper ocean response to an applied wind stress. To accommodate the latitudinal extent of the model, spherical coordinates are used, with ϕ (longitude) increasing eastward and θ (latitude) increasing northward. Eastward and northward upper layer transport components are defined by $U = uH$ and $V = vH$, respectively, where u, v are the depth-independent upper layer ϕ, θ velocity components and H is the upper layer thickness. The equations are

$$\frac{\partial U}{\partial t} + \frac{1}{a\cos\theta}\frac{\partial}{\partial\phi}\left(\frac{U^2}{H}\right) + \frac{1}{a}\frac{\partial}{\partial\theta}\left(\frac{UV}{H}\right) - (2\Omega\sin\theta)V = \frac{-g'}{2a\cos\theta}\frac{\partial H^2}{\partial\phi} + \frac{\tau^{(\phi)}}{\rho_1} + A\nabla^2 U \quad (1a)$$

$$\frac{\partial V}{\partial t} + \frac{1}{a\cos\theta}\frac{\partial}{\partial\phi}\left(\frac{UV}{H}\right) + \frac{1}{a}\frac{\partial}{\partial\theta}\left(\frac{V^2}{H}\right) + (2\Omega\sin\theta)U = \frac{-g'}{2a}\frac{\partial H^2}{\partial\theta} + \frac{\tau^{(\theta)}}{\rho_1} + A\nabla^2 V \quad (1b)$$

$$\frac{\partial H}{\partial t} + \frac{1}{a\cos\theta}\left[\frac{\partial U}{\partial\phi} + \frac{\partial}{\partial\theta}(V\cos\theta)\right] = 0 \quad (1c)$$

where $g' = g(\rho_2 - \rho_1)/\rho_2$ is the reduced gravitational acceleration, a is the Earth's radius, Ω is the Earth's rotation rate, A is a kinematic eddy viscosity, and wind stress $\tau = \{\tau^{\phi}, \tau^{\theta}\}$ is applied as a body force over the upper layer [*Charney*, 1955].

Model geometry, shown in Figure 1, simulates the geography of the Arabian Sea from 40°E to 73°E and from 10°S to 25°N. Boundary conditions along all solid boundaries are nonslip. Open boundaries are located along the entire southern boundary and along the eastern boundary from 5°S to the equator. Boundary conditions here are a variation of the Sommerfeld radiation condition as described by *Camerlengo and O'Brien* [1980]. Solid boundaries are located along all remaining boundaries, including the southeastern corner of the model, which simulates the Chagos Archipelago; the region from the equator to the Gulf of Khambat, which simulates the Laccadive and Maldive islands; and the shallow bank regions around the Seychelles and Socotra. Narrow, deep channels within island chains are ignored.

The model equations are solved numerically on a 135 × 74 finite difference mesh which is staggered in space. Model resolution is 1/8° zonally ($\Delta\phi$) and 1/4° meridionally ($\Delta\theta$). The equations are integrated in time using a leapfrog finite difference scheme, with a forward time difference used every ninety-ninth time step to eliminate the computational mode.

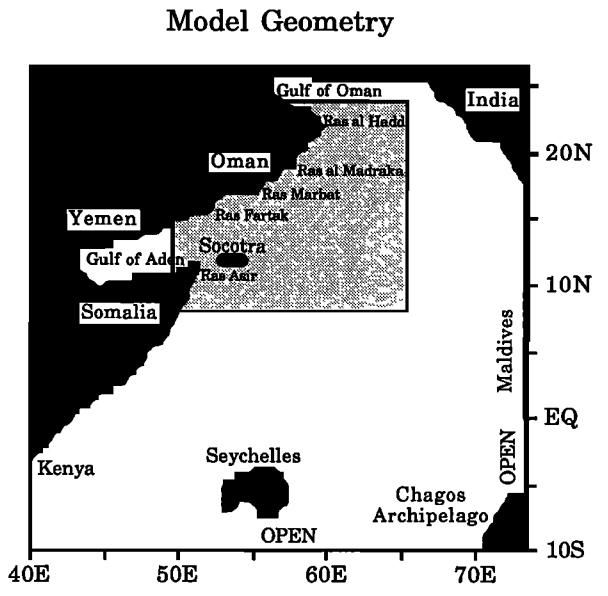

Fig. 1. Model geometry. Black areas indicate land boundaries. Significant geographic features surrounding the Arabian Sea, including major islands of Socotra, the Seychelles, Laccadives, Maldives, Chagos Archipelgo, and surrounding shoals, are represented as solid land masses. The straits of Hormuz and Bab-al-Mandab are assumed closed, while open boundaries exist along the southern boundary at 10°S and the eastern boundary from 5°S to the equator. The stippled area indicates the region of this study.

The model time step is 30 min. In the linearized form of the reduced gravity equations, linear phase speed for the particular baroclinic mode to be modeled, $C = (g'H_0)^{1/2}$, must be prescribed. In the nonlinear form used here, there is no analogous phase speed parameter, only g'; however, in the numerical solution of the model equations, initial upper layer thickness H_0 must be defined. This is analogous to prescribing an initial phase speed, although it does not remain constant, as variations of H are large with respect to H_0. Average upper layer thickness varies owing to inflow and outflow through the open boundaries during the seasonal cycle. The other free parameter in the model is A, the kinematic eddy viscosity, which serves to damp out grid-scale noise in the model and prevents this noise from growing through nonlinear interactions. It is chosen as low as possible while maintaining numerical stability.

For results presented here, $H_0 = 200$ m, $A = 0.75 \times 10^3$ m^2 s^{-1}, and $g' = 0.03$ m s^{-2}. The model was integrated from rest, beginning at 0001 UT on December 16, 1984, using an exponential taper with an e-folding time of 20 days to reduce the initial transients. The monthly mean winds for 1985 were applied repeatedly for 4 years until a steady seasonal cycle was obtained. The results presented here are from the fourth year of the simulation. For simplicity, the model year is 360 days, with each month containing 30 days.

THE DATA

Wind Forcing

The model is forced by wind observations obtained from the National Climatic Data Center, Asheville, North Carolina. Wind observations are extracted from the raw data and consist of marine surface wind observations originating from merchant ships, buoys, research vessels, and other ocean measurement stations, for the region 30°E to 122°E and 26°S to 26°N. Approximately 10,000–20,000 observations are available per month.

The raw wind data are first converted to pseudostress by the objective analysis procedure, developed and discussed in detail by *Legler et al.* [1988]. Each observation's pseudostress, τ, is initially calculated by

$$\tau^* = \mathbf{W}|\mathbf{W}| \tag{2}$$

where $\mathbf{W}$ is the wind velocity. These pseudostress values are filtered to remove obviously erroneous reports. The remaining reports are then binned into 1° latitude × 1° longitude blocks and filtered a second time with respect to the standard deviation of all the reports in each individual block. Typically, less than 1% of the total reports are eliminated from the data set by these two filtering processes, but significant data gaps, generally located off standard shipping lanes, still exist. A typical filtered pseudostress chart for September 1985 is shown in Figure 2. The remaining empty blocks in the filtered fields are assigned values through bilinear interpolation, while grid points over land are assigned values by extrapolating the marine data, so that the gradient of the vector values normal to the coastal boundaries is zero.

The next step in the wind analysis involves minimizing a functional on the observations, climatology, and final pseudostress values using the conjugate-gradient method of *Navon and Legler* [1987]. This minimization technique results in final pseudostress values that in a least squares sense are close to the filtered data values, with curl and divergence close to the observations and to the climatological values for the region from *Hellerman and Rosenstein* [1983]. The final pseudostress fields calculated for actual wind data from the fall of 1985 are shown in Figures 3–5. For this study, these pseudostress fields are converted to wind stress by the bulk aerodynamic formula

$$\tau = \rho_a C_D \tau^*$$

where ρ_a is the density of air and C_D is a constant drag coefficient. For the results presented here, $\rho_a = 1.2$ kg m^{-3} and $C_D = 1.25 \times 10^{-3}$. These values provide reasonable upper layer transports, consistent with a number of observations [e.g., *Leetmaa et al.*, 1982; *Swallow et al.*, 1983; *Schott*, 1983].

Corroborative Data

During the fall of 1985, U.S. Navy ships in the Arabian Sea collected XBT readings, while NOAA 8 and 9 spacecraft imaged the regions surrounding Socotra and off the coast of the Arabian Peninsula. For this study, 353 XBT readings and 20 AVHRR channel 3, 4, and 5 satellite images were obtained covering the area from 8°N to 23°N and 50°E to 65°E. These data are analyzed to determine the oceanographic features present in the northwest Arabian Sea during September–November 1985. These features are then used to verify the accuracy of the fall 1985 model output resulting from the realistic wind data used to force the model.

XBT data are received from the Navy in standard Navy message format and are decoded to extract date, time, position, temperature, and depth information, which is then used to plot geographic positions and temperature versus depth profiles. Because of geographic limitations in the available data (approximately 150 of the 183 September XBT

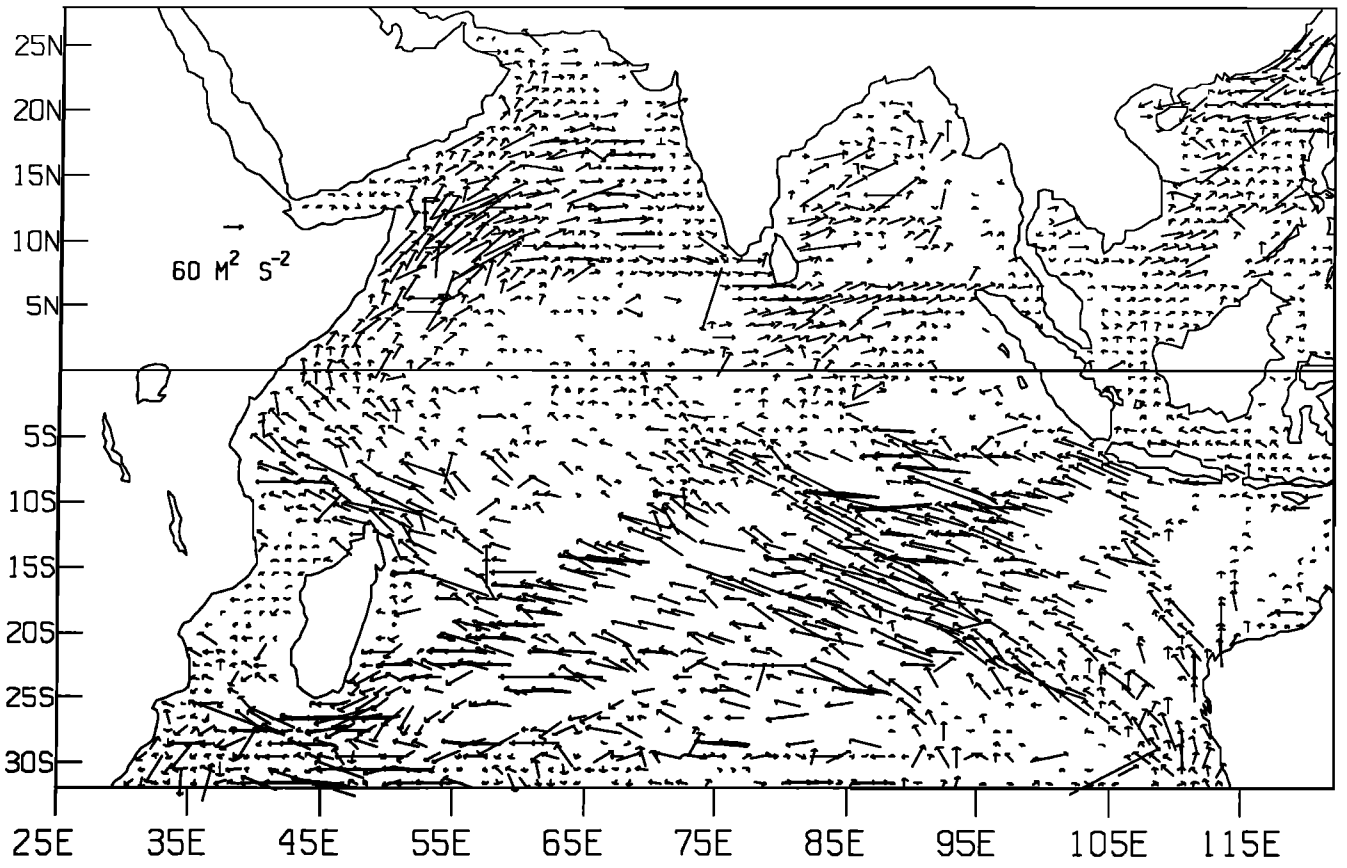

Fig. 2. Filtered pseudostress for September 1985. Arrows indicate direction and magnitude with units of $m^2 s^{-2}$. The chart is derived from wind observations and has been filtered to remove obviously erroneous reports. Large gaps exist, generally located off standard shipping lanes, but the area around and to the north of Socotra is well covered. Note the region of high pseudostress around and to the southeast of Socotra.

readings were taken off the coast of Oman, while about 120 of the 170 October readings were taken around the island of Socotra) two charts are developed, one bounding the region 13°N to 23°N and 58°E to 66°E, which contains the September XBT readings, and the other bounding the region 8°N to 18°N and 50°E to 60°E, which contains the October XBT readings. Temperature versus depth profiles are then used to determine an isotherm that provides a reasonably accurate representation of the thermocline depth for the two regions. The 20° isotherm is most representative of the thermocline depth for the September data, while the 18° isotherm best represents the October thermocline depth. The readings are separated into six 10-day increments extending from September 1–10 to October 20–30, and each XBT is plotted at its correct geographic position on the appropriate 10-day chart. The six charts were then hand contoured, based upon the 20°C (September) or 18°C (October) isotherm depth. The chart for October 10–20 is shown in Figure 6.

AVHRR satellite images of the Arabian Sea covering the period August 30 to November 30, 1985, were provided by the Scripps Satellite Oceanography Facility. Owing to the recording schedule for the satellites, only daytime passes were available during the time frame of this study. A number of the images were contaminated by monsoonal moisture (channel 4) and by sun glint (channel 3), but sufficient images were acceptable to determine many of the significant oceanographic features present during the period. A sample image from the NOAA 9 pass of November 2, 1985, is shown in Figure 7. In subsequent analyses, we consider only the quantity ΔSST of deviations about the mean sea surface temperature (SST) from the AVHRR data. Since we are comparing these data to model upper layer thickness, it is only the patterns of SST variability that are of interest, i.e., the location of fronts and eddies; therefore rather than a precise calibration of absolute SST we need only its gradients, which are more easily obtained.

RESULTS

Preface

The emphasis of this study is focused on the transition period between the breakdown of the southwest monsoon and the spin-up of the northeast monsoon during September–November 1985 for the northwest Arabian Sea, around and north of Socotra. Figure 8, showing the October 16, 1985, model output, introduces the dynamic features discussed throughout the study. Three anticyclonic eddies (the great whirl, south of Socotra; Socotra Eddy, east of Socotra; and the North Socotra Warm Eddy, north and northwest of Socotra) and one cyclonic eddy (the North Socotra Cold Eddy, northeast of Socotra) dominate the dynamic features around Socotra, while to the north, along the Arabian peninsula, a large relatively homogeneous thin upper layer structure extends from immediately along the coast to well offshore. It is assumed throughout that high values of model upper layer thickness (ULT) are indicative of a deeper

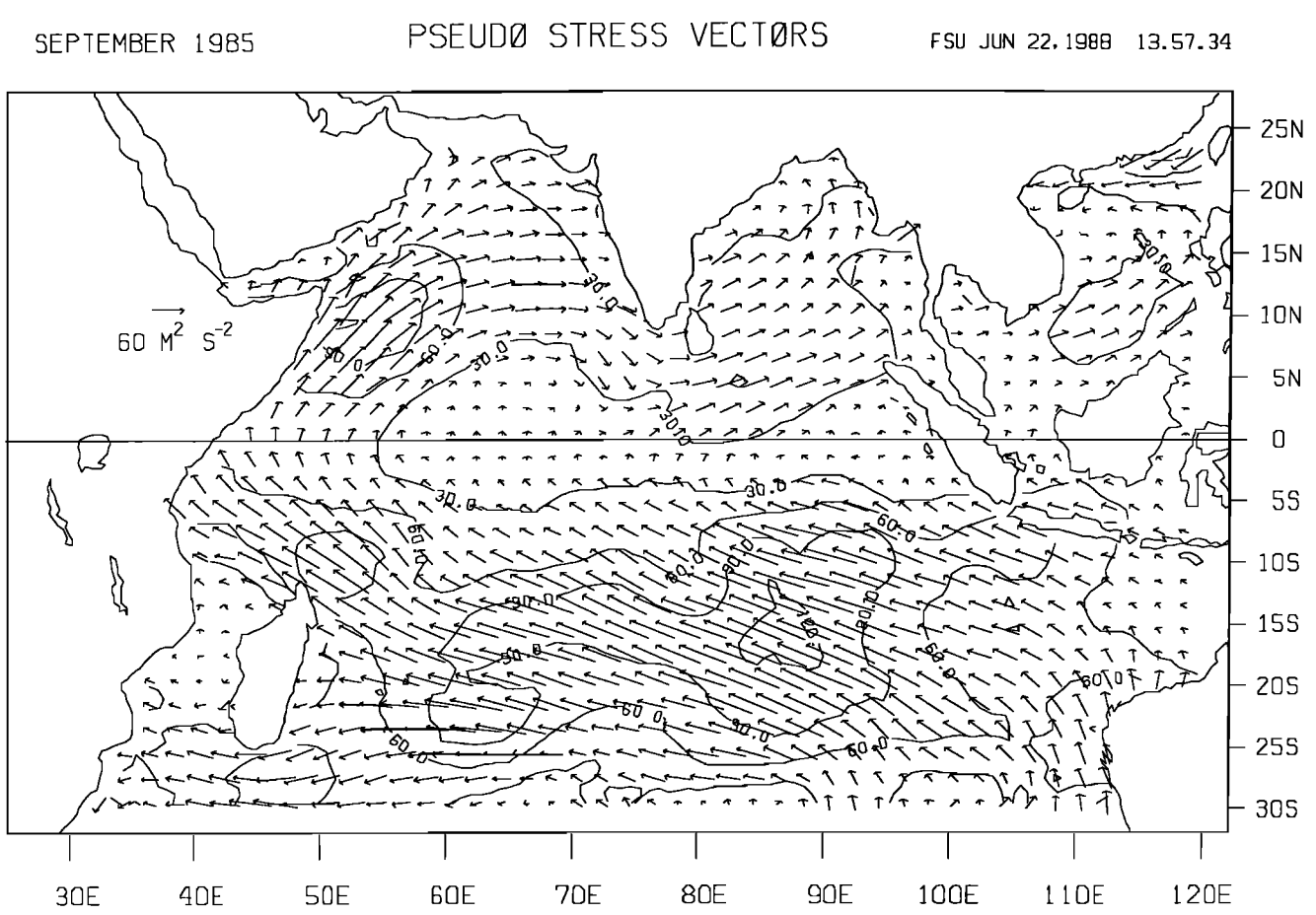

Fig. 3. Resultant pseudostress for September 1985. These data are computed by bilinearly interpolating the filtered pseudostress data of Figure 2 to fill in empty regions, and then determining pseudo-stress values by the conjugate-gradient minimization process developed by *Legler et al.* [1988]. Arrows again provide direction and magnitude of the pseudostress in units of $m^2 s^{-2}$. Contours provide a visual interpretation of regions of high and low pseudostress. Note the region of strong southwesterly pseudostress to the south-southeast of Socotra.

thermocline and higher SST, while lower values of ULT correspond to a shallower thermocline and cooler SST.

1985 Response to Observed Wind Forcing

The 1985 model response to observed wind forcing is generated by repeatedly applying the observed 1985 monthly mean winds to the model for 4 years, until a steady seasonal response to the shifting monsoon winds is obtained. Focusing on the region from 8°N to 23°N and 50°E to 65°E, the oceanic response during the winter months reflects a general breakdown of the energetic eddy field that was established in the previous year.

By mid-December there is no sign of the great whirl to the south of Socotra. It has been replaced by the southward flowing winter Somali Current, which is fed from the Sverdruplike interior to the south and east of Socotra. Remnants of the North Socotra Warm and Cold eddies are present in mid-January (Figure 9), with central ULT of 215 m and 140 m, respectively. A very weak clockwise flow is seen on the east coast of Socotra. Another weak warm-core eddy is present off Oman to the northeast of the North Socotra Cold Eddy, with a central ULT of 212 m located at 68°E, 17°N. These two warm eddies are the remnants from the breakup of the previous year's Socotra Eddy. A broad, weak clockwise flow is located in the north central Arabian Sea, between 62° and 66°E and 18° and 25°N. This anticyclonic eddy propagates westward and intensifies as it reaches the coast of Oman in March and April. In April and May this eddy coalesces with the northern remnant of the Socotra Eddy, and the resulting circulation gradually decays until late August, when it can no longer be seen. The remnants of the North Socotra Warm and Cold eddies, in contrast, decay very rapidly and can no longer be seen by early April.

In June, with the onset of upwelling favorable southwest monsoon winds, a narrow band of upwelling, 50 to 100 km wide with ULT of 150 to 160 m, forms along the coast from Somalia to Ras al Hadd. A narrow alongshore, northeastward current is associated with this upwelling band. The great whirl begins to form south of 8°N and is embedded in a broad gyre that is forming across the central and western Arabian Sea. This gyre forms in response to the wind stress curl pattern associated with the southwest monsoon winds, with the Somali Current as its western boundary current and the great whirl as a recirculation in this western boundary current. Weak flow leaves the Somali Current and passes between Socotra and Ras Asir.

As the Findlater Jet moves northward and strengthens in July, the great whirl intensifies and also moves northward, reaching 9°–10°N by mid-July (Figure 10). A wedgelike feature of decreased ULT forms just to the north of the great whirl along the Somali coast, with intense upwelling between the great whirl and the coast. Outflow from the great whirl

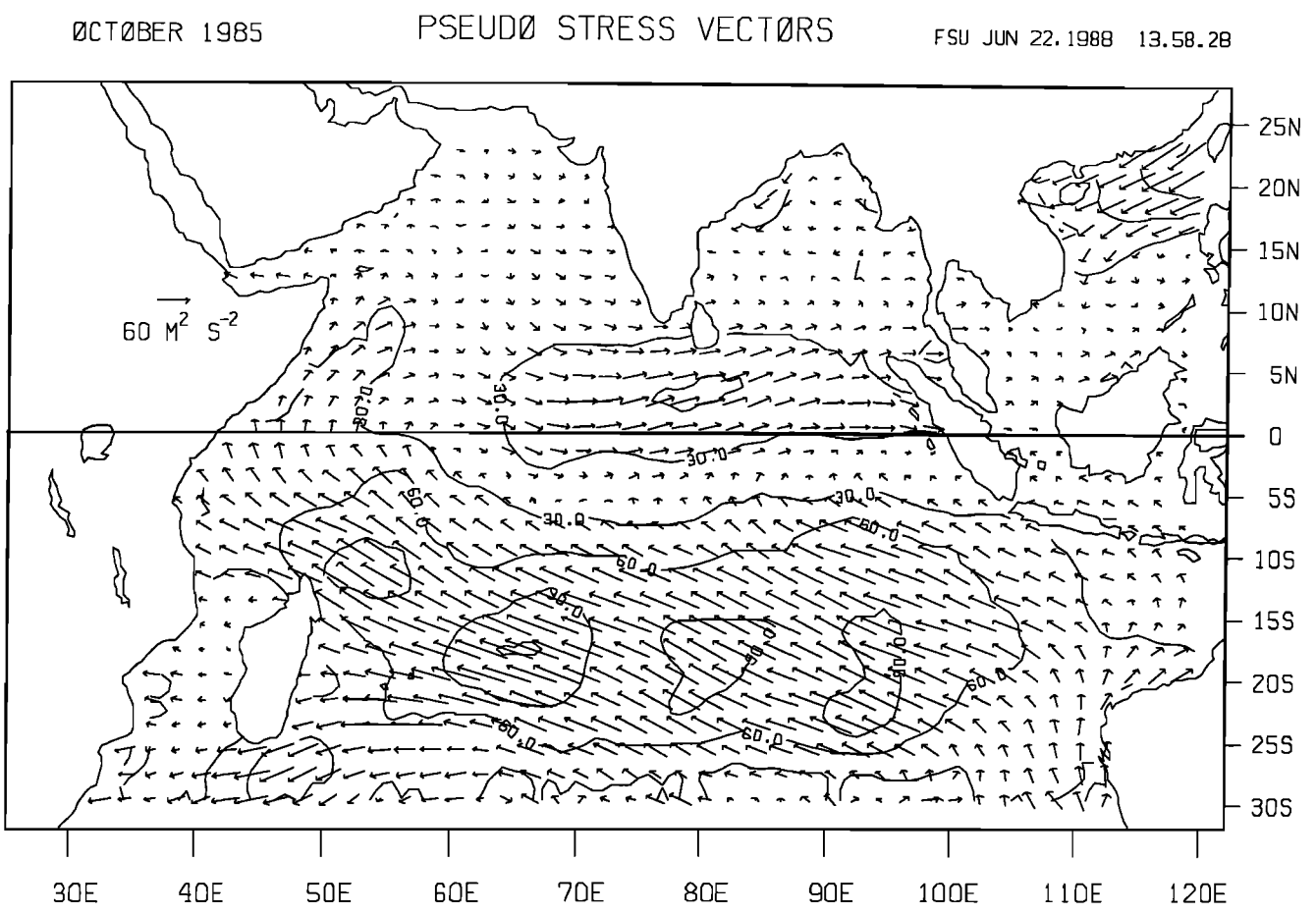

Fig. 4. Same as Figure 3, but for October 1985. Values around and to the north of Socotra have diminished significantly, and direction reversal has begun.

splits at 10°–11°N, with part flowing to the northwest around the wedge and through the passage between Ras Asir and Socotra, and part flowing eastward into the interior of the gyre. A broad band of upwelling forms along the Arabian Peninsula, extending 400 km from the coast, in response to the strong positive wind stress curl to the northwest of the Findlater Jet axis.

The Findlater Jet and its associated curl field begin to relax in late July and early August. At this time, the broad upwelling band begins to break up into several large eddies (Plate 1). (Plate 1 is shown here in black and white. The color version can be found in the separate color section in this issue.) The great whirl impinges on the south coast of Socotra, with central depths exceeding 275 m. Flow from the great whirl through the passage west of Socotra increases. This flow continues northward to the Yemen coast, where it then turns to the east and forms large meanders. This flow pattern was reported in a British pilot atlas by *Findlay* [1866]. By mid-September these meanders have formed two closed circulations, the clockwise North Socotra Warm Eddy to the north of Socotra and the anticlockwise (cyclonic) North Socotra Cold Eddy to the northeast. Outflow to the east of the great whirl begins to form a second recirculation that is separated from the great whirl by a tongue of low ULT. This second recirculation becomes the Socotra Eddy described by *Bruce* [1979], although it is weaker in 1985 than in most years (see below). The cold tongue intensifies in late August and early September, forming a closed eddy that moves southward around the eastern edge of the great whirl, while the Socotra Eddy moves northward. A pulse of high ULT propagates westward as a Rossby wave from the interior between 12° and 14°N (Figure 11), arriving at 57°E in early September and causing an intensification of the Socotra Eddy. A cold tongue, or ridge on the thermocline, extends southward from the North Socotra Cold Eddy and continues to separate the Socotra Eddy from the coast of Socotra. This pattern intensifies through October, with another closed, anticlockwise circulation forming between the great whirl and the Socotra Eddy in the lee of the island of Socotra.

Through late November and into December, with the onset of the northeast monsoon winds, the great whirl is destroyed as an area of low ULT and southwestward current propagates westward from the interior at 0.1 m/s, which is approximately the speed of a Rossby wave at this latitude. This southwestward flow reaches the coast by mid-December and becomes the winter Somali Current. The Socotra Eddy moves to the north around the North Socotra Cold Eddy to the coast of Oman. These three remaining eddies contract to the northwest and decay gradually through the winter months, and the cycle described earlier is repeated.

Climatological Assessment

To determine the significance of the oceanographic dynamic structure in this region for 1985 with respect to other years, two additional model cases are considered: one forced by observed interannual winds analyzed by *Cadet and Diehl* [1984] from the period 1954–1976, and the other forced by

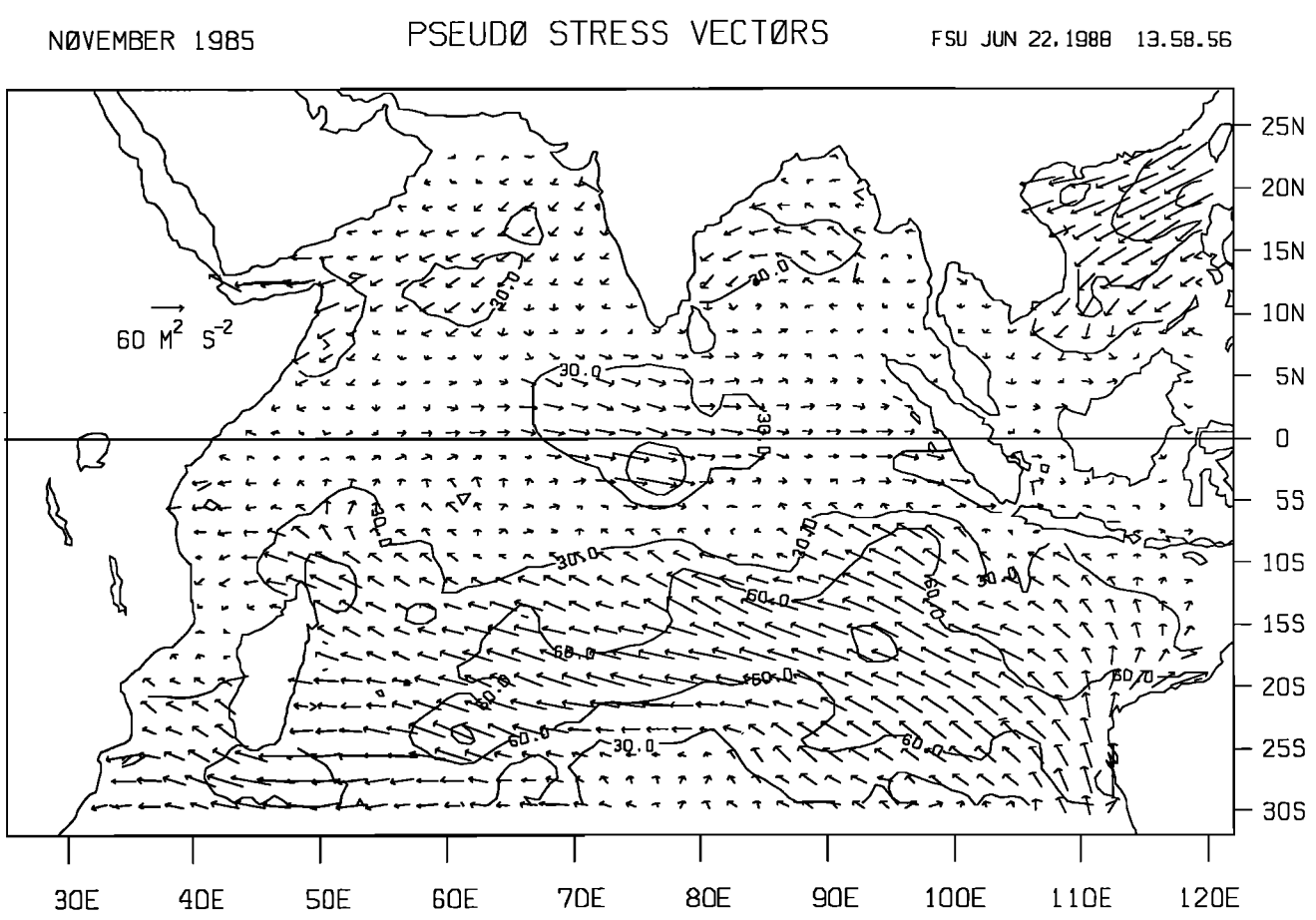

Fig. 5. Same as Figure 3, but for November 1985. Direction has reversed north of the equator and maxima from the northeast begin to form to the east and southwest of Socotra.

monthly mean climatological winds from the same 23-year period. These results are compared with the 1985 results forced by observed winds, to determine the unique features, if any, present in 1985.

Although no 2 years display the exact same structure in the interannual case, two reasonably consistent patterns frequently appear. One, in which the great whirl, Socotra Eddy and North Socotra Warm Eddy appear, occurs in 13 of the 23 years (1954, 1956, 1958, 1961–1968, 1971, and 1972), while the other, in which the North Socotra Warm Eddy is absent from the system, occurs in the remaining 10 years (1955, 1957, 1959, 1960, 1969, 1970, and 1973–1976). The year 1954, a year of relatively strong monsoon winds, and 1973, a year of relatively weak monsoon winds, are most representative of the two

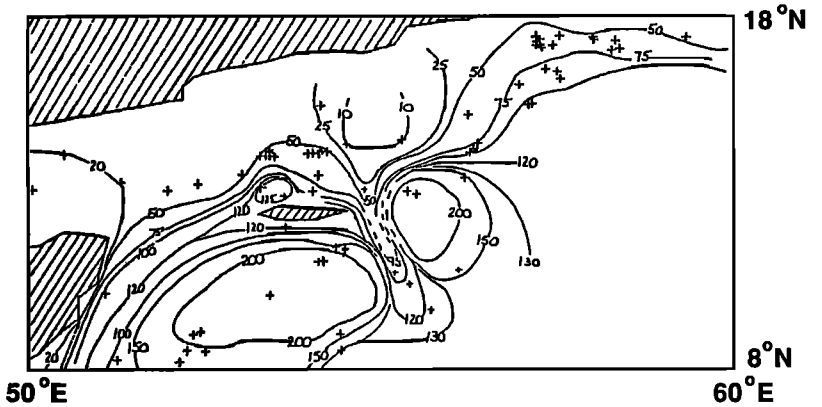

Fig. 6. The 18°C isotherm depth (meters) for October 10–20, 1985. Contours are generated from XBT data obtained by the U.S. Navy over the 10-day period, for which depth profiles indicated that the 18°C isotherm best represented the thermocline depth. Dashed lines indicate regions of deficient XBT readings and are estimated contours. Three anticyclonic eddies appear to the south, east, and northwest of Socotra, and a cyclonic eddy appears to the northeast with an attached tongue of cool water penetrating to the south along the eastern shore of Socotra. Strong fronts appear off the Somali coast and between the four dominant eddies.

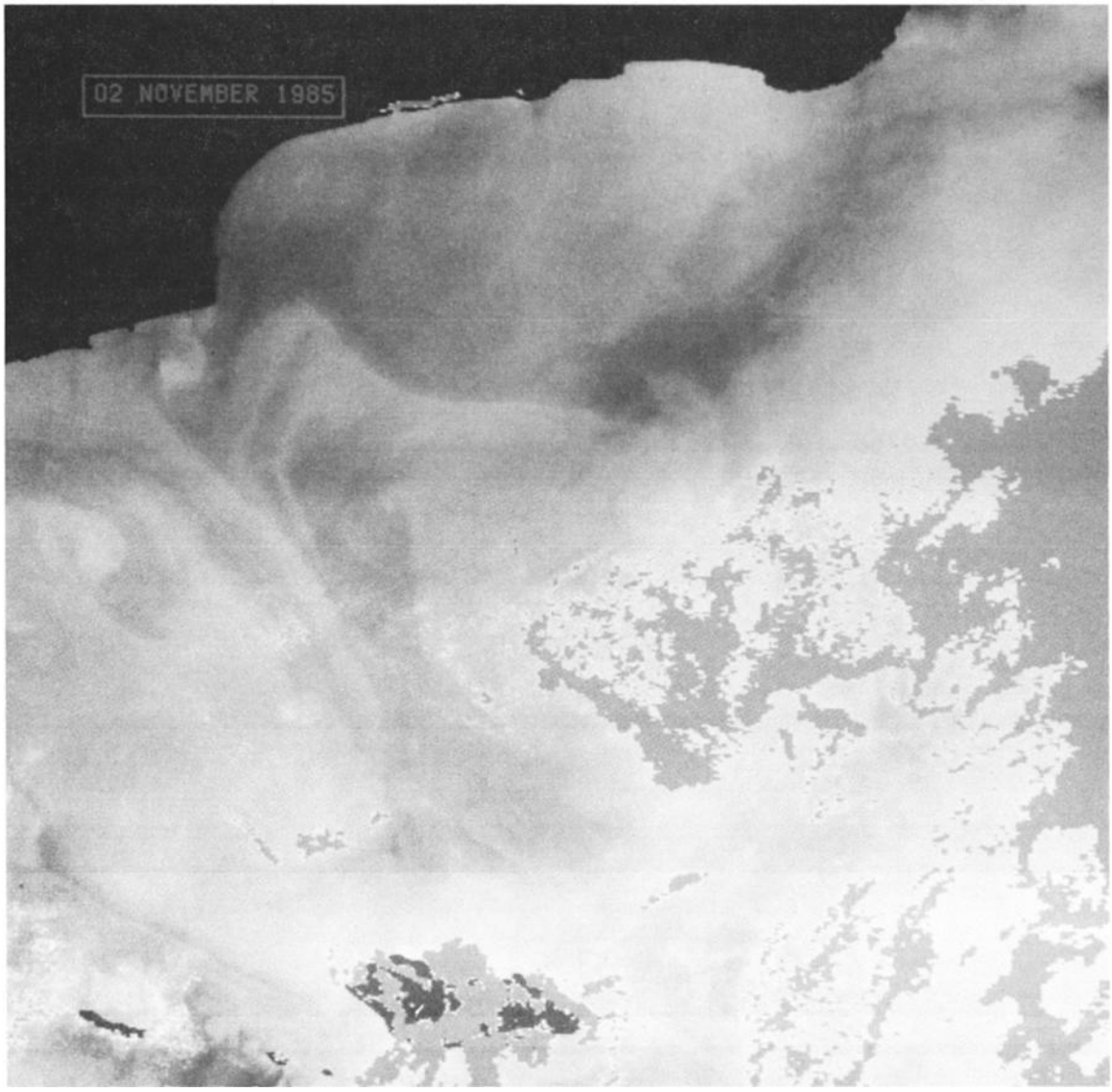

Fig. 7. NOAA 9 AVHRR image of November 2, 1985, for the region between Socotra and the Arabian Peninsula. Socotra is located at the bottom center of the image, while Yemen extends along the top. Warm surface temperature, indicative of anticyclonic flow, can be recognized by the lightly shaded region north and northwest of Socotra, while cooler water, indicated by the darker shading, is observed in the upper center of the image, south of and offshore of the Arabian Peninsula between Ras Fartak and Ras Marbat.

patterns and are shown in Figures 12 and 13. The climatological wind case is also shown in Figure 14. This case is very different from both the 1954 and 1973 cases. As in 1973, the North Socotra Warm Eddy is absent. Both it and the Socotra Eddy are replaced by a single warm eddy, elongated in the zonal direction, to the north and northeast of Socotra. The cold tonguelike feature seen in 1954, which is missing in 1973, is replaced by a very intense cold eddy to the east of Socotra and the great whirl in the climatological case. These differences can be explained in part by differences in the strength of the wind field. In 1954 the Findlater Jet was stronger and narrower, and its axis was located farther to the north than in 1973, giving it a more southerly component. The stronger winds drive a more inertial Somali Current, giving rise to more intense eddy formation in 1954. In the climatological case, the interannual variability in the position and strength of the jet gets smeared, resulting in a more diffuse jet and a less inertial Somali Current.

Comparison of these three cases with the 1985 case reveals that 1985 was, in fact, a relatively unique year. The well-developed Socotra Eddy in September, the cold tongue east of Socotra in October, and the absence of the two anticyclonic flows along 61°E for the entire period are all significant deviations from what is normally observed in the model. Figure 15, a profile of the 1985 case and climatological case for October 16 across 14°N, graphically demonstrates the departure of the 1985 dynamics from the climatological response. Hence 1985 did indeed provide a unique opportunity to assess dynamic features relatively uncommon in the region; i.e., the model is not merely simulating climatology.

Model Assessment

Late August and early September mark the beginning of the active eddy development observed in the fall around

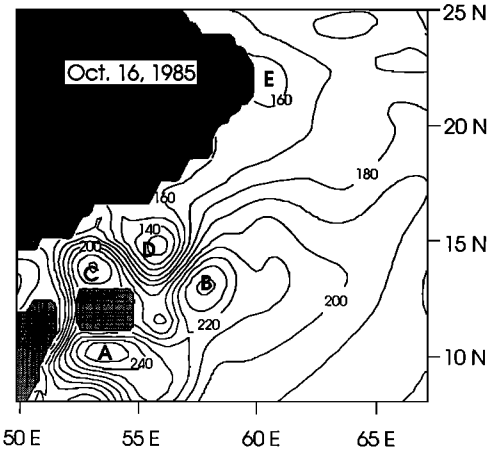

Fig. 8. Model response (ULT) for October 16, 1985, forced by observed winds. Four prominent eddies appear around Socotra: the anticyclonic great whirl to the south (A), the Socotra Eddy to the east (B), the North Socotra Warm Eddy to the northwest (C), and the cyclonic North Socotra Cold Eddy to the northeast (D). Farther north, a large homogeneous region of low ULT exists off the coast of Oman (E). The contour interval is 10 m.

Socotra and farther to the north along the coast of the Arabian Peninsula. At the beginning of September, formation of the North Socotra Warm Eddy dominates the dynamics around Socotra. Closed anticyclonic flow, with its associated high ULT, is observed to the northwest of the island, while a region of low ULT extends south from the Arabian Peninsula to the northeast of the island. Plate 2, a NOAA 8 satellite SST image for August 30, confirms the presence of warmer water of the North Socotra Warm Eddy along the northwestern edge of Socotra and cooler water located to the northeast. (Plate 2 is shown here in black and white. The color version can be found in the separate color section in this issue.) In Figures 16 and 17 it can be seen from profiles along 14°N and 15°N of satellite ΔSST and model response for September 1 that these two distinct features are properly positioned by the model. While it is difficult to compare amplitudes between ΔSST and ULT, the patterns are consistent. The front between 55°E and 56°E is accurately positioned by the model, but the minimum in ΔSST is farther to the east than the minimum in ULT.

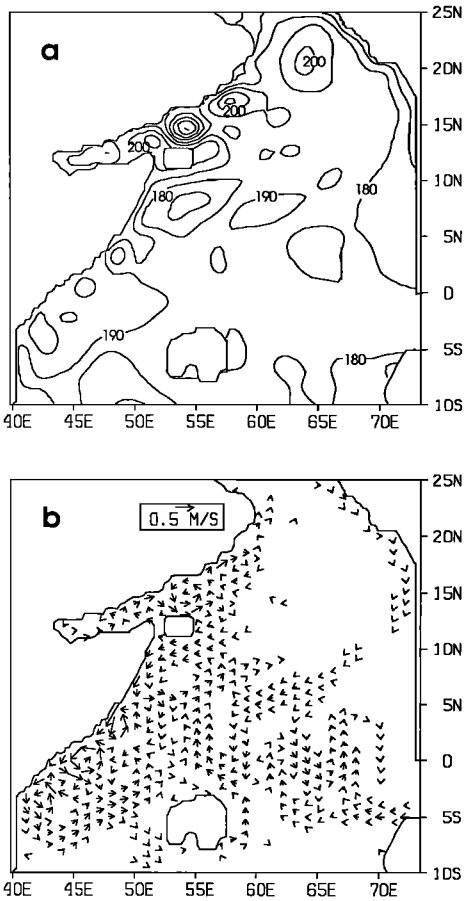

Fig. 9. Circulation for January 16, 1985, from the model. (*a*) ULT in meters. The contour interval is 10 m. (*b*) Upper layer velocity. Arrows indicate magnitude and direction. Velocities of less than 0.05 m s^{-1} are suppressed. Arrows are shown only once per degree in both directions for clarity of display.

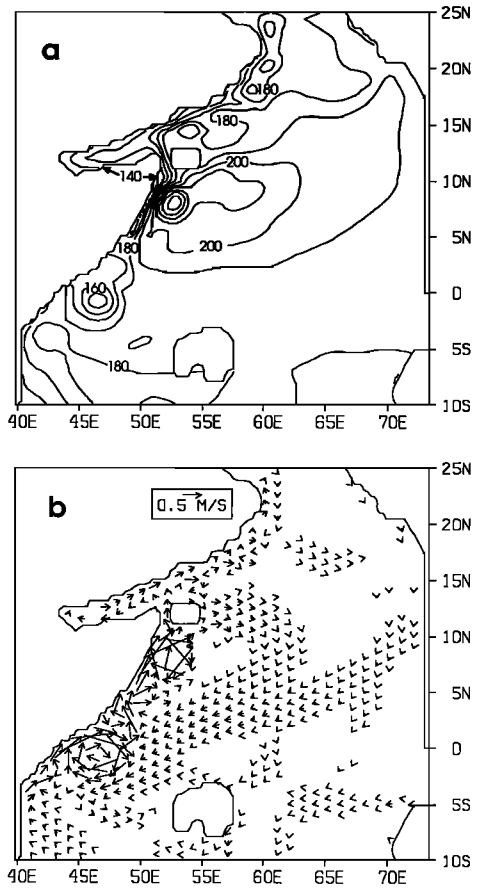

Fig. 10. Same as Figure 9, but for July16, 1985.

Along the coast of the Arabian Peninsula, a large band of lower ULT exists, extending eastward to about 65°E. This feature, along with a trace of the warm eddy from the previous year at about 20°N, is present in the region in early to mid-September and appears in both the model response and the XBT data of mid-September (Figure 18). A profile comparison along 21°N for this date (Figure 19) shows the warm region off the coast, followed by the large region of low ULT and cooler water farther to the east. A feature noticeably absent from the model, however, is the region of upwelling that extends approximately 50–60 km immediately off the coast in the XBT data. This failure of the model to predict the thin zone of coastal upwelling along the Omani coast occurs throughout September in the model results and

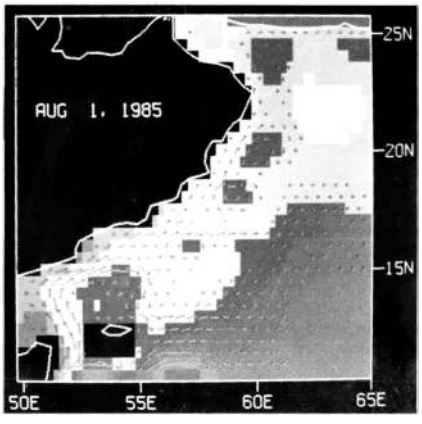

Plate 1*a*

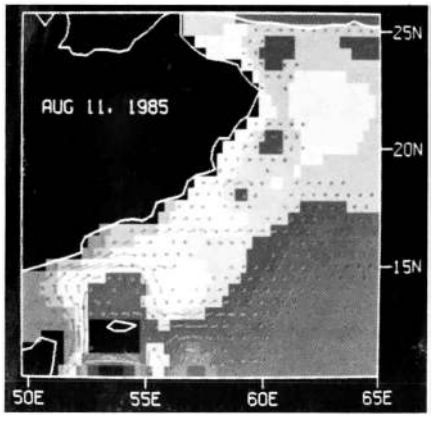

Plate 1*b*

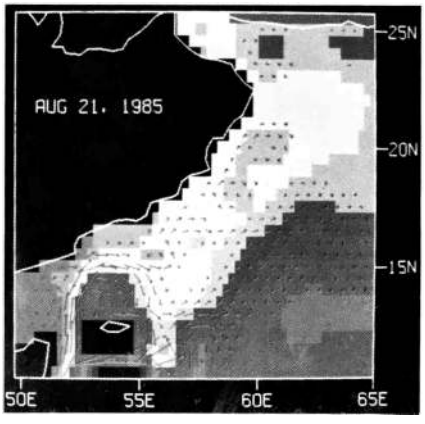

Plate 1*c*

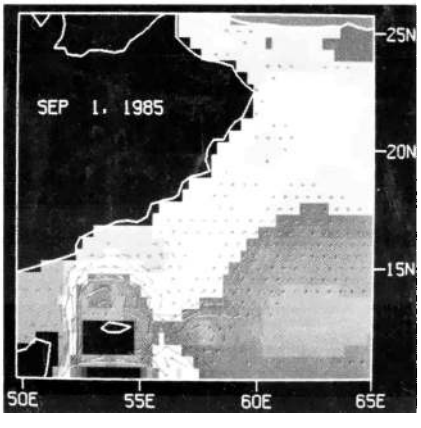

Plate 1*d*

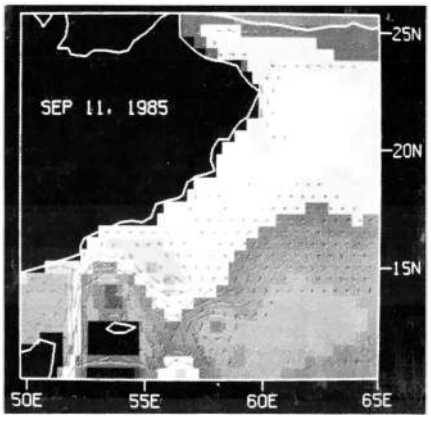

Plate 1*e*

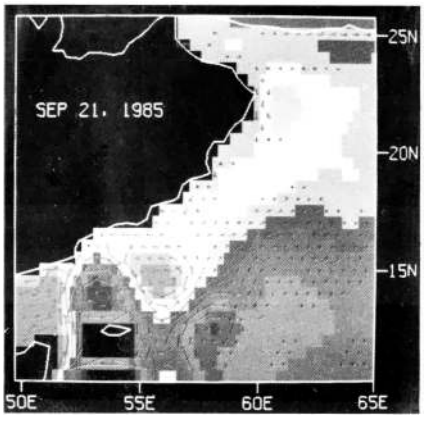

Plate 1*f*

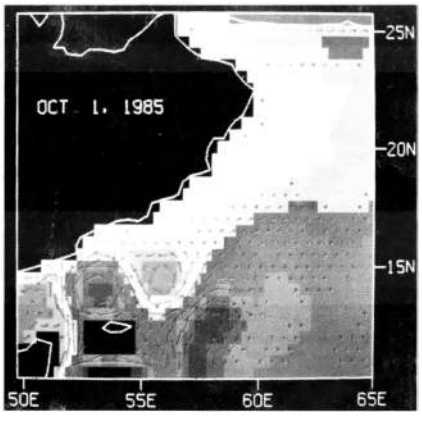

Plate 1*g*

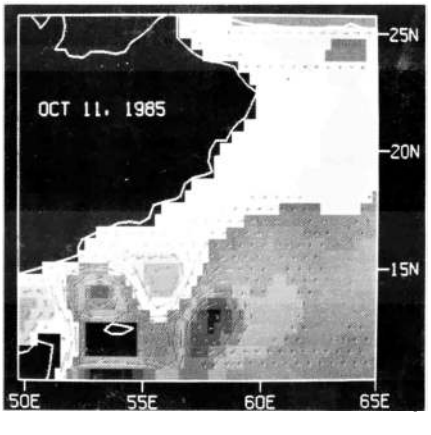

Plate 1*h*

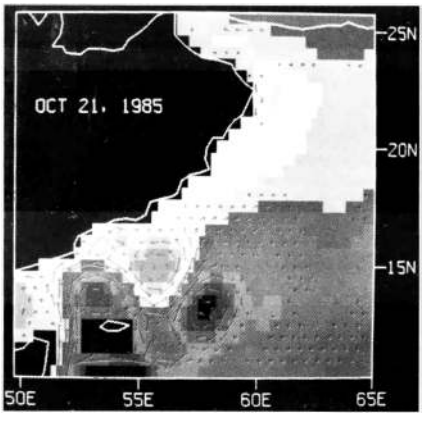

Plate 1*i*

Plate 1. Formation of the eddies around Socotra. Model fields are shown every 10 days from August through October for the northwestern corner of the model basin. Arrows show upper layer velocity, with only two arrows shown per degree in both directions. Velocities of less than 0.05 m/s are surpressed and velocities larger than 0.8 m/s truncated to 0.8 m/s for clarity. The great whirl forms to the south of this region in late June under the direct influence of the Findlater Jet, and moves northward in late July until it impinges on the south coast of Socotra. Some outflow from the great whirl passes through the channel between Socotra and Ras Asir, while additional outflow continues eastward and meanders into the interior (Plates 1*a*–1*c*). The North Socotra Warm and Cold eddies form in early September in the meandering outflow from the channel west of Socotra (Plates 1*d*–1*f*). The Socotra Eddy initially forms in the outflow east of the great whirl (Plate 1*a*) and then moves northward and intensifies as it merges with an area of high ULT that propagates westward from the interior as a Rossby wave (Plates 1*c*–1*f*). A tongue of low ULT separates the Socotra Eddy from the coast. This cold tongue forms to the northeast of the great whirl (Plate 1*b*) and is advected around the great whirl to the southeast (Plates 1*c*–1*g*). (The color version and a complete description of this figure can be found in the separate color section in this issue.)

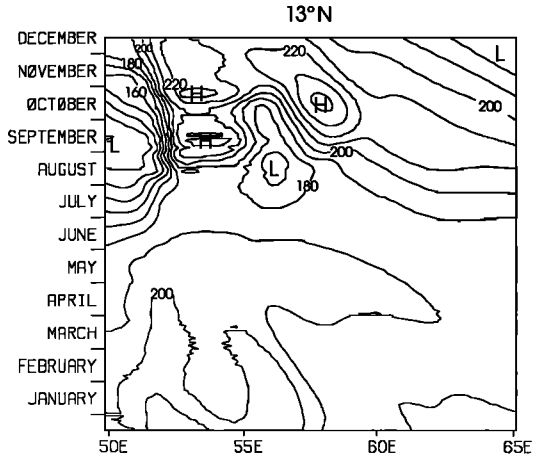

Fig. 11. Time-longitude plot of ULT across 13°N from 50°E to 65°E. East of 62°E, ULT deepens from June through late August in response to negative wind stress curl, reaching a maximum in late August. Increasing ULT propagates westward from this region as downwelling Rossby waves at 0.1 m/s, as evidenced by the sloping contours of ULT between 57°E and 62°E. In late August this Rossby wave pulse reaches the longitude of the Socotra Eddy and causes an intensification of this eddy, which is seen as the high at 58°E in October. The cold tongue that separates the Socotra Eddy from the coast of Socotra is seen as the low at 56°E. The north coast of Socotra is located between 53°E and 55°E one grid point to the south of this section. The southern edge of the North Socotra Warm Eddy is seen as the highs in this longitude range in September and October. The upwelling in the mouth of the Gulf of Aden is seen in the low ULT west of 52°E in June through November. In early September, upwelling Rossby waves are seen propagating into the region west of 65°E from farther to the east, excited by the changing wind stress curl in the interior of the Arabian Sea.

appears to be a deficiency either in the model or in the winds used to force the model. The latter is most likely the case, since the model is capable of resolving upwelling on this scale. It is likely that the nearshore winds driving the coastal upwelling were not adequately sampled in the ship-observed winds used in our analysis.

Throughout the remainder of September, the region off the Omani coast (for which the majority of September XBT data

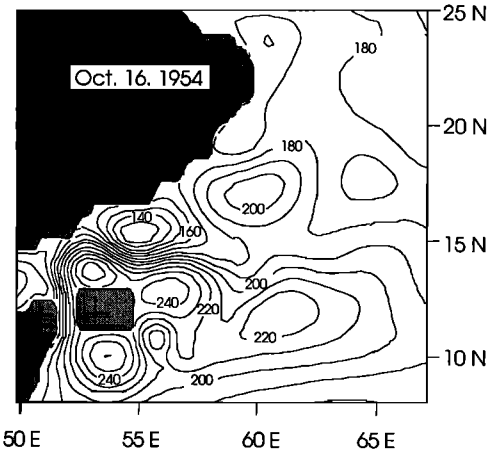

Fig. 12. Model response for October 16, 1954, forced by observed interannual winds. Representative of a year of strong monsoon winds in which the three major anticyclonic eddies appear around Socotra, the great whirl, Socotra Eddy, and North Socotra Warm Eddy are present, but two additional anticyclonic eddies occur along 60°E, one at 12°N and the other at 17°N. The North Socotra Cold Eddy is present, but the cold tongue is separated from it and appears as a cyclonic eddy to the southeast of the island.

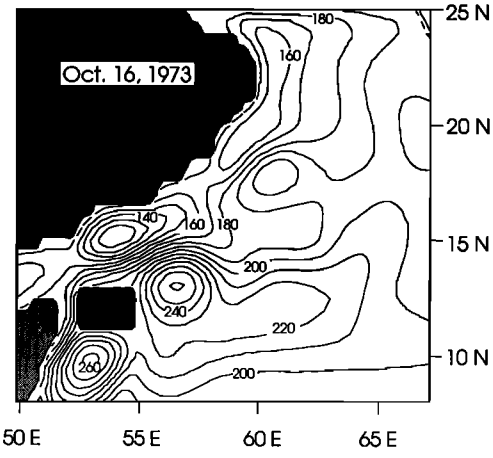

Fig. 13. Model response for October 16, 1973, forced by observed winds. Representative of a year in which monsoon winds were anomalously weak and only two of the major anticyclonic eddies occur around Socotra, the great whirl and Socotra Eddy appear, but the North Socotra Warm Eddy is absent. Again, two additional anticyclonic eddies are present along 61°E at 12°N and 17°N. The North Socotra Cold Eddy is elongated against the coast with weak, elongated cold eddies off the Oman coast and in the Gulf of Aden.

exist) remains relatively constant in structure in both the model and the XBT data. Again, the data clearly display an upwelling region immediately off the coast, which is absent from the model. To the south, around Socotra, XBT data are insufficient to distinguish dynamic features during September.

As can be seen in Figure 8, the model shows October to be the most dynamically active month for the region surrounding Socotra. The remnants of the great whirl to the south, the North Socotra Warm Eddy to the northwest, the North Socotra Cold Eddy to the northeast, and the Socotra Eddy to the east all display very active patterns and provide numerous flow and frontal characteristics upon which a comp arison of the model and the available XBT and satellite data can be conducted.

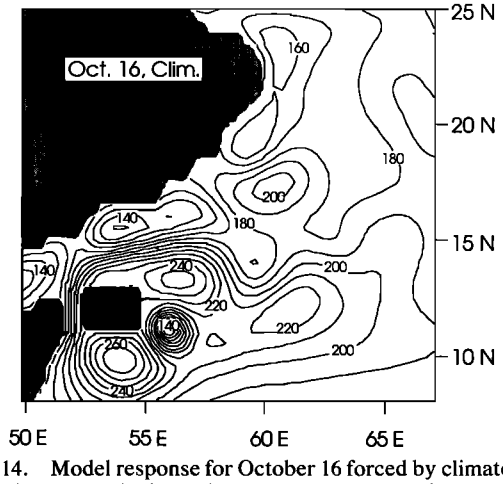

Fig. 14. Model response for October 16 forced by climatological winds. Five anticyclonic eddies occur: the great whirl, the Socotra Eddy, a weak North Socotra Warm Eddy, and two eddies along 61°E at 12°N and 17°N. Cyclonic eddies, in addition to the North Socotra Cold Eddy along the Arabian Peninsula, occur southeast of Socotra and along 60°E at about 14°N, 19°N, and 23°N. Elongated weak, cold eddies appear off Oman and in the Gulf of Aden.

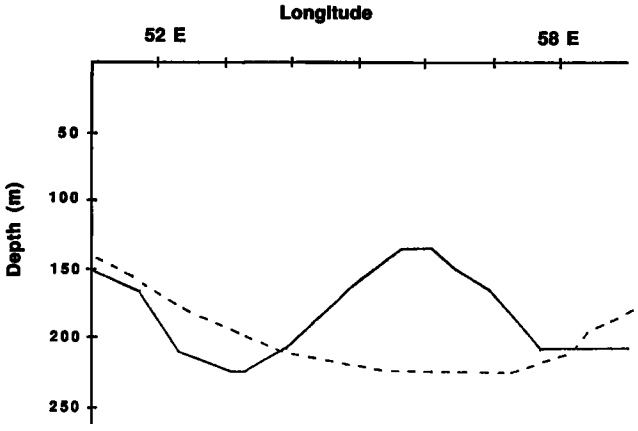

Fig. 15. Upper layer profiles for the case forced by 1985 observed winds (solid line) and the case forced by climatological winds (dashed line) for October 16, 1985, along 14°N. The North Socotra Warm Eddy at about 53.2°E and Socotra Eddy at about 57.8°E are distinctly separated by the North Socotra Cold Eddy at about 55.8°E in the 1985 case. In the climatological case the two anticyclonic eddies have coalesced into one large eddy with maximum depth attained at about 56°–57°E.

Plate 2. The NOAA 8 AVHRR image of August 30, 1985, for the region south of the Yemen coast. Socotra is in the lower left corner of the image. (The color version and a complete description of this figure can be found in the separate color section in this issue.)

The XBT data for October 1–10, contoured in Figure 20, show the great whirl, Socotra Eddy, and North Socotra Cold Eddy, as well as an indication of the North Socotra Warm Eddy which in fact is present, as satellite imagery for this period confirms. Significantly, it also shows the low-ULT tongue extending south from the North Socotra Cold Eddy along the eastern shore of Socotra. As previously discussed, this is a unique feature of 1985 and is clearly present in the model result for October 11 (Plate 1). In Figure 21, profiles of the region to the south of Socotra display the similarity of the model to the data in simulating the great whirl's position and spatial dimension. In the model, the cold tongue is weaker and displaced slightly to the east, while the great whirl is broader than in the observations. The front at 51°E appears somewhat steeper in the observations.

Toward the end of the month, there is an expansion to the northwest of the North Socotra Warm Eddy and slow westward drift, toward Socotra, of the Socotra Eddy. This latter effect is apparent in the October 21 model response, by the breakdown of the cool tongue east of Socotra into a

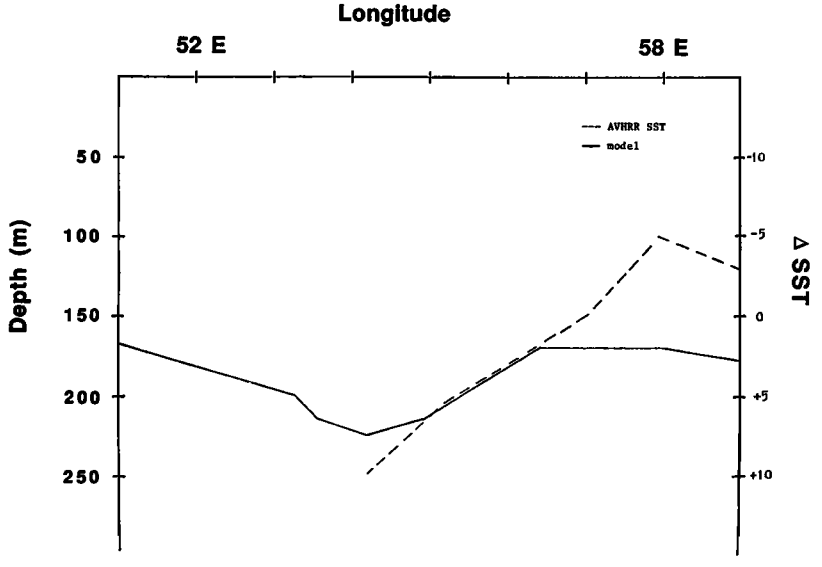

Fig. 16. Profiles of the sea surface temperature anomalies from the NOAA 8 AVHRR image of August 30, 1985 (dashed line), and the model ULT for September 1, 1985 (solid line), along 14°N. AVHRR data are available between 54°E and 59°E and have been averaged on 1° blocks. The cold tongue extending south from the North Socotra Cold Eddy is apparent in both profiles between 57°E and 58°E. Likewise, the North Socotra Warm Eddy is apparent in each, with a maximum depth at about 54°E.

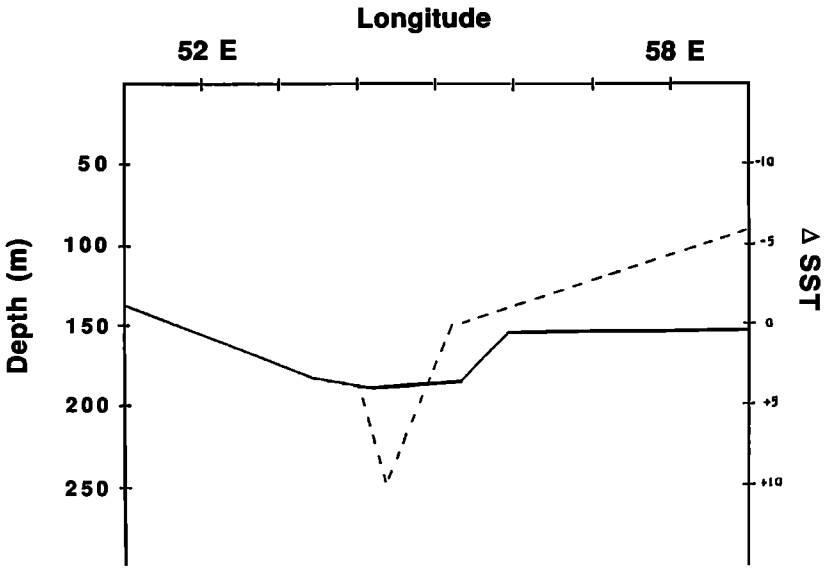

Fig. 17. Same as Figure 16, but along 15°N. Again, the North Socotra Warm Eddy appears properly placed by the model, reaching a maximum at about 54.2°E.

strong frontal boundary to the north and a small cyclonic eddy to the south (Plate 1). The contoured XBT data for October 20–30 (Figure 22) show this effect as the cool tongue contracts in the center, pinching off a small eddy to the south. Again, profiles of the model response and XBT data along 14°N (Figure 23) demonstrate a remarkable similarity between the model and the observations. The locations of the fronts and eddies do not exactly coincide, although the patterns follow one another quite closely. The North Socotra Warm Eddy is properly located by the model but appears stronger in this section. The front between the North Socotra Warm Eddy and the North Socotra Cold Eddy is similarly located in both model and observations, although the North Socotra Cold Eddy and the Socotra Eddy are displaced to the east by about 50 km in the model.

For November the model displays a slow weakening of the dynamic features developed during the fall. The two cyclonic and three anticyclonic eddies established in the previous months maintain their respective positions throughout November, but all show signs of spreading and weakening as the pycnocline flattens. Strong fronts remain along the Gulf of Aden and between the North Socotra Cold Eddy and the Socotra and North Socotra Warm Eddies, but the great whirl and weak cyclonic eddy southeast of Socotra deteriorate significantly and are almost indistinguishable by the end of the month.

In Figure 24 the NOAA 9 satellite sea surface temperature image of November 2 is compared with the November 2 model response along 14.5°N. The resulting profiles again show the accurate placement of the North Socotra Warm Eddy, North Socotra Cold Eddy, Socotra Eddy, and associated frontal boundaries separating these features. Again, it is the similarity of the patterns in ΔSST and ULT, not their amplitude, that is important. The size of the eddies and the width of the frontal zones separating them appear consistent between the model and the observations.

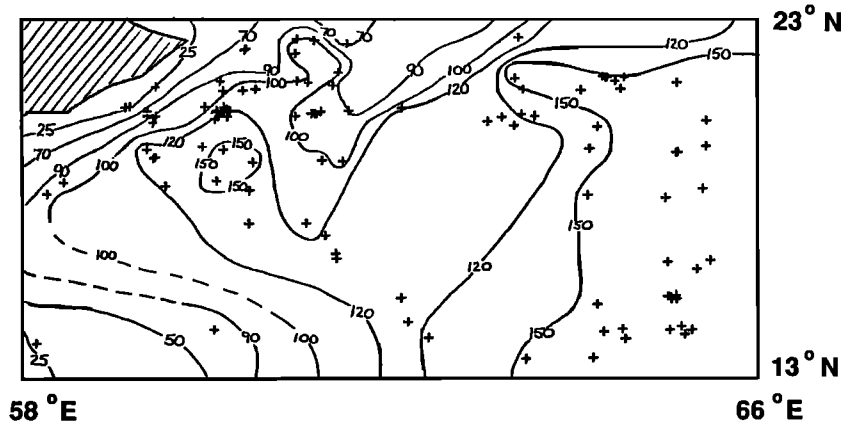

Fig. 18. The 20°C isotherm depth (meters) for September 10–20, 1985. Dashed lines indicate regions where XBT data are deficient and contours are estimated. Upwelling persists off the Omani coast, with ULT increasing with distance from shore. A shallow (cool) tongue penetrates from the north at about 19°N between 61°E and 62°E, while indications of a small anticyclonic eddy appear centered at about 19°N, 60.5°E.

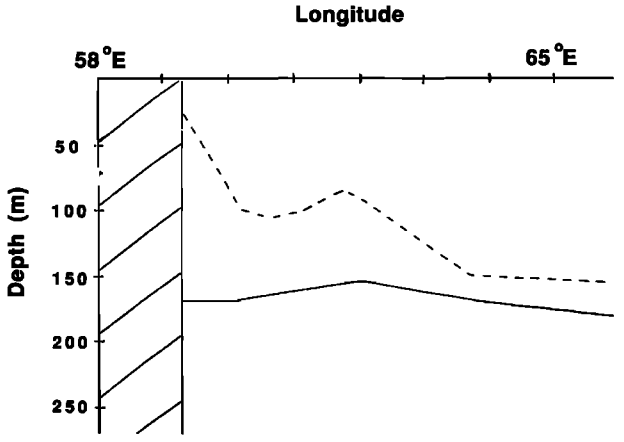

Fig. 19. Profiles of the XBT 20°C isotherm depth for September 10–20, 1985 (dashed line), and model ULT for September 16, 1985 (solid line), along 21°N, with the coast of the Arabian Peninsula extending over the first 130 km. The XBT data clearly show a 50- to 60-km region of upwelling immediately off the coast of Oman, which is absent from the model response.

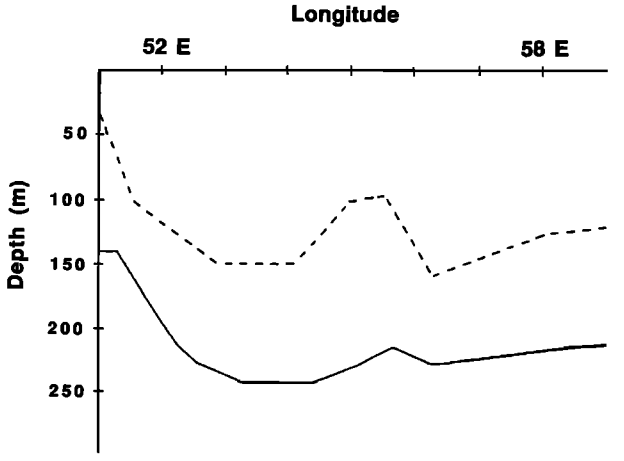

Fig. 21. Profiles of the XBT 18°C isotherm for October 1–10, 1985 (dashed line), and the model ULT for October 6, 1985 (solid line), along 10°N. The strong front off of Somalia is observed east of 52°E, followed by the great whirl at 52°–55°E and the Socotra Eddy at about 56°–57°E, separated by the cold tongue at 55°–56°E.

Discussion and Conclusions

This study has confirmed that the fall circulation pattern of the northwest Arabian Sea is strongly influenced by the transition of the region from the regime of the summer southwest monsoon to that of the winter northeast monsoon. The strong eddies and fronts generated during July and August, at the height of the southwest monsoon, persist throughout the period and respond to the influence of the rapidly reversing winds and surface current.

Throughout the study, in which forcing was provided by 1985 observed winds, the model has proven quite effective in its ability to reproduce the upper layer ocean structure observed in 1985. In particular, around Socotra, a region dominated by robust features (the great whirl to the south, the Socotra Eddy to the east, the North Socotra Cold Eddy to the northeast, and the North Socotra Warm Eddy to the northwest), the model compares well with the observational data, with each of the four principle eddies well represented both spatially and temporally. Off the coast of Oman, however, where the oceanic structure is characterized by relatively weak flows and a narrow band of coastal upwelling, the model is less effective. Small-scale structures overlying the dominant gradual increase of ULT with offshore distance, while clearly evident in the observational data, are absent from the model. Instead, the model represents the area as a large region of relatively constant ULT. Model resolution, which is approximately 30 km at this latitude, in conjunction with the weak nature of the flow, probably is responsible for much of the model's difficulty here. The absence of the upwelling band in the model results is most likely due to poorly resolved coastal winds in the model forcing field; however, coastal topography, which in reality varies dramatically from a wide shelf between Ras al Hadd and Ras Marbat to a very narrow shelf to the south of Ras Marbat, probably plays a significant role in the presence and structure of this upwelling. Again, this effect is not represented in the model. Similarly, the effects of thermodynamics may also serve as a potential source of error, as the summer-heated waters of the Persian Gulf and Gulf of

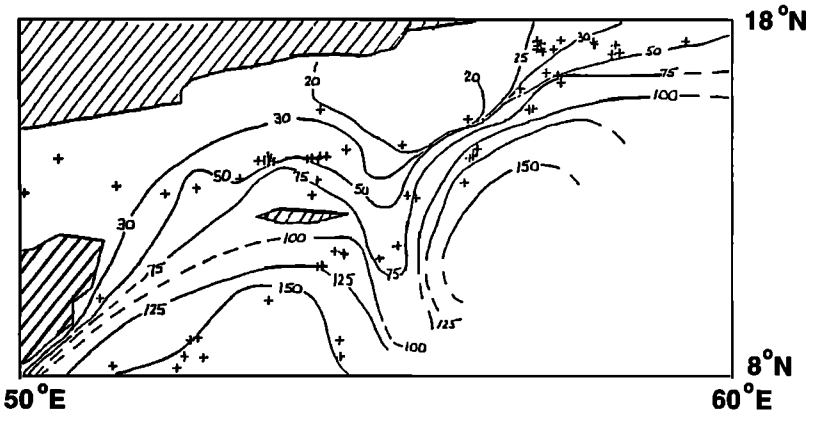

Fig. 20. The 18°C isotherm depth (meters) for October 1–10, 1985. Contours are generated from the XBT data (solid contours) when sufficient readings are available and are estimated (dashed contours) where XBT data are deficient. The great whirl is seen penetrating from the south, while indications of the Socotra Eddy are observed in a deepening of the isotherm east of Socotra. The strong North Socotra Cold Eddy is observed to the northeast of Socotra, with a relatively cool tongue extending to the south immediately east of the island and separating the great whirl and Socotra Eddy. Increasing ULT is observed to the north and west of Socotra, while intense fronts are observed off the coast of Somalia, northeast of Socotra, and between the Socotra Eddy and the intense North Socotra Cold Eddy.

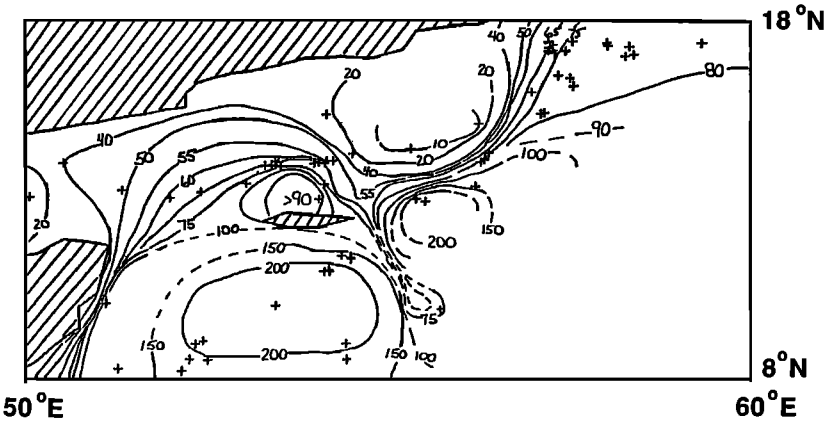

Fig. 22. The 18°C isotherm depth (meters) for October 20–30, 1985. Contours are generated from the XBT data (solid contours) when sufficient readings are available and are estimated (dashed contours) where XBT data are deficient. The intense great whirl maintains itself to the south of Socotra, while the Socotra Eddy continues to slowly migrate to the west. The North Socotra Warm Eddy has intensified and expanded to the northwest, almost touching the Arabian Peninsula. The North Socotra Cold Eddy has also expanded and intensified, while the cool tongue to the east of Socotra is almost pinched off. Strong fronts occur off the coast of Somalia; between the North Socotra Warm Eddy, North Socotra Cold Eddy, and Socotra Eddy; to the east of the North Socotra Cold Eddy; and off the east coast of Socotra.

Oman, (where September SST frequently exceeds 30°C) likely impart an influence on the continuity of the upper layer structure off the Omani coast. This is also not accounted for in the model, though it probably is less important than the resolution and topography effects.

Regardless, the fluctuations observed in the data off the Omani coast are quite small, of the order of tens of meters over the entire 750,000-km^2 region, and when compared with the robust features found around Socotra, they appear to be of only minor significance. Hence the model does provide a very reasonable hindcast of the dynamic structure observed in the fall of 1985.

Further model improvement is both possible and desirable. As was discussed above, inclusion of coastal topography and thermodynamic effects may vastly improve the model's accuracy in regions of weak flow and relatively constant horizontal structure. Additionally, the expansion of the model geometry to include the entire Indian Ocean basin (now implemented in other versions of the model) should improve the model's results, as remote forcing, particularly from the southern hemisphere trade winds, will exert a greater influence on the model response. Multilevel vertical structure would also be useful in determining vertical shearing and entrainment effects on the upper layer circulation (multilayer and multilevel versions of the model are under development).

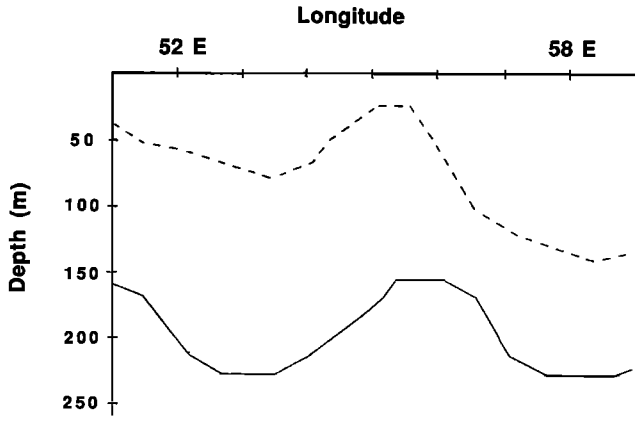

Fig. 23. Profiles of the XBT 18°C isotherm for October 20–30, 1985 (dashed line), and model ULT for October 26, 1985 (solid line), along 14°N. The cool water of the Gulf of Aden, the North Socotra Warm Eddy (52°–54°E), North Socotra Cold Eddy (55°–56°E), and Socotra Eddy (57°–59°E) are clearly evident in each profile. The three strong frontal boundaries separating these four major features also appear in both profiles.

A number of recommendations can be made to enhance further verification studies. Of foremost concern in any assessment must be the availability of corroborating data. While the limited data available for this study were sufficient, coverage of specific areas of interest would have both simplified and improved the analysis; for example, better XBT coverage east of Socotra could have improved the analysis of the cool tongue present east of Socotra in the model in October. Better satellite AVHRR coverage would have been helpful in delineating many of the observed features as well. Finally, verification studies should be attempted when drifters, buoys, phytoplankton, and other observational data are all available concurrently. This requires close interaction between modelers and observationalists to ensure a unified and successful effort.

Better resolution, both in space and in time, in the observed wind fields used to force the model will most certainly improve such simulations. The availability of scatterometer winds in the future will provide this increased resolution; however, even scatterometer winds are not accurate near coastal areas and would not help the model to resolve the narrow upwelling band observed off of Oman in the fall of 1985.

Despite the limited resources available, this study has provided a useful insight into the model's effectiveness and is an important evolutionary step in the model's development. It has shown the ability of this simple $1\frac{1}{2}$-layer model to reproduce accurately the robust features of the Arabian Sea when provided accurate observed wind data, and it justifies further model improvement and sophistication. More importantly, it has demonstrated the ability of the model to use near real-time winds to reproduce accurately Arabian Sea dynamics and sets the stage for the possible forecasting in

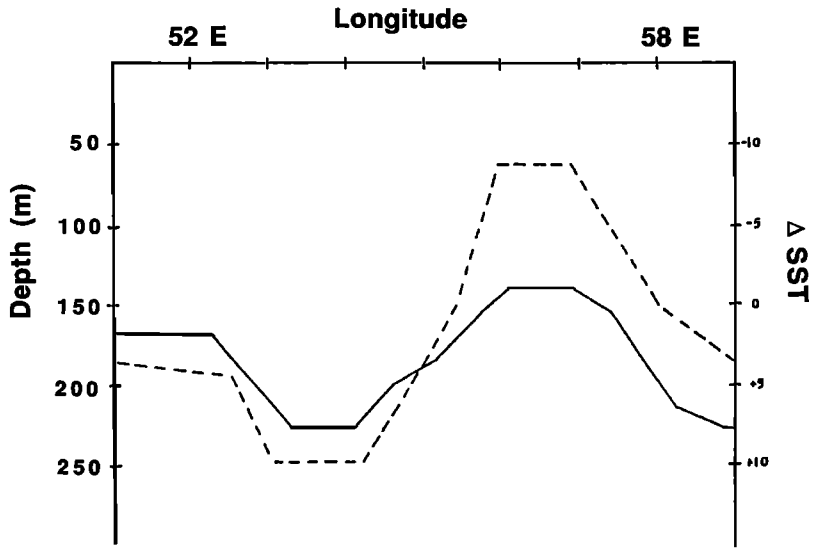

Fig. 24. Profiles depicting sea surface temperature anomalies averaged on 1° blocks from the NOAA 9 AVHRR image of November 2, 1985 (dashed line), and the model upper layer depth for November 2, 1985 (solid line), along 14.5°N. Again, the curves show the North Socotra Warm Eddy at about 53°–55°E, the North Socotra Cold Eddy at 55°–58°E, the Socotra Eddy east of 58°E, and strong frontal boundaries separating these features.

near real time of the region's ocean dynamics when scatterometer winds become available early in the next decade.

Acknowledgments. Modern ocean modeling has evolved to the point where a consolidated effort on the part of many is necessary to achieve success. Thus we wish to express our gratitude to the many individuals who participated and assisted us with this project. Support was provided by the Office of Naval Research (ONR) through the Secretary of the Navy Research Chair in Oceanography and the Institute for Naval Oceanography. Supplemental support was provided by the NASA Oceanic Processes Branch as part of the NASA Traineeship Grant. TOGA wind data were provided by NOAA. This research was supported in part by the Florida State University (FSU) through time granted on its Cyber 205 supercomputer. We thank FSU for providing us access to this computer. The FSU Supercomputer Computations Research Institute is funded by the Department of Energy. Thanks to B. J. Cagle of the ONR Western Regional Office, who provided the motivation for this work and arranged for the Navy XBT data, R. Whritner of the Scripps Satellite Oceanography Facility, who provided the satellite SST imagery, and I. M. Navon, who was instrumental in the development of the objective analysis used on the wind data. Thanks also to the anonymous reviewers for their constructive criticism. We wish to express our appreciation to Rita Kuÿper for her masterful performance during the tedious typing phase of the project. Geophysical Fluid Dynamics Institute contribution 269; Supercomputer Computations Research Institute contribution 70.

REFERENCES

Anderson, D. L. T., The Somali Current, *Ocean Modelling*, *34*, 6–9, 1981.

Anderson, D. L. T., and D. W. Moore, Cross-equatorial jets with special relevance to very remote forcing of the Somali Current, *Deep Sea Res.*, *26*, 1–22, 1979.

Anderson, D. L. T., and P. B. Rowlands, The Somali Current response to the monsoon: The relative importance of local and remote forcing, *J. Mar. Res.*, *34*, 395–417, 1976.

Brown, O. B., J. G. Bruce, and R. H. Evans, Evolution of sea surface temperature in the Somali Basin during the southwest monsoon of 1979, *Science*, *209*, 595–597, 1980.

Bruce, J. G., Large scale variations of the Somali Current during the southwest monsoon, *Deep Sea Res.*, *20*, 837–846, 1973.

Bruce, J. G., Eddies off the Somali coast during the southwest monsoon, *J. Geophys. Res.*, *84*(C12), 7742–7748, 1979.

Bruce, J. G., The wind field in the western Indian Ocean and the related ocean circulation, *Mon. Weather Rev.*, *111*, 1442–1452, 1983.

Cadet, D. L., and B. C. Diehl, Inter-annual variability of surface fields over the Indian Ocean during recent decades, *Mon. Weather Rev.*, *112*, 1921–1935, 1984.

Cagle, B. J., and R. Whritner, Arabian Sea project of 1980—Composites of infrared images, technical report, pp. 1–61, West. Reg. Off., Off. of Nav. Res., Pasadena, Calif., 1981.

Camerlengo, A. L., and J. J. O'Brien, Open boundary conditions in rotating fluids, *J. Comput. Phys.*, *35*, 12–35, 1980.

Charney, J. G., The generation of ocean currents by the wind, *J. Mar. Res.*, *14*, 477–498, 1955.

Cox, M. D., A mathematical model of the Indian Ocean, *Deep Sea Res.*, *17*, 47–75, 1970.

Cox, M. D., Equatorially trapped waves and the generation of the Somali Current, *Deep Sea Res.*, *23*, 1139–1152, 1976.

Cox, M. D., A numerical study of Somali Current eddies, *J. Phys. Oceanogr.*, *9*, 311–326, 1979.

Cox, M. D., A numerical study of surface cooling processes during summer in the Arabian Sea, in *Monsoon Dynamics*, edited by M. J. Lighthill and R. P. Pearce, pp. 529–540, Cambridge University Press, New York, 1981.

Evans, R. H., and O. B. Brown, Propagation of thermal fronts in the Somali Current system, *Deep Sea Res.*, *28*, 521–527, 1981.

Findlater, J., Mean monthly airflow at low levels over the western Indian Ocean, *Geophys. Mem.*, *115*, 53 pp., 1971.

Findlay, A. G., *A Directory for the Navigation of the Indian Ocean*, 1062 pp., Richard Holmes Laurie, London, 1866.

Hellerman, S., and M. Rosenstein, Normal monthly wind stress over the world ocean with error estimates, *J. Phys. Oceanogr.*, *13*, 1093–1104, 1983.

Hurlburt, H. E., and J. D. Thompson, A numerical model of the Somali Current, *J. Phys. Oceanogr.*, *6*, 646–664, 1976.

Knox, R. A., and D. L. T. Anderson, Recent advances in the study of low-latitude ocean circulation, *Prog. Oceanogr.*, *14*, 259–318, 1985.

Leetmaa, A., D. R. Quadfasel, and D. Wilson, Development of the flow field during the onset of the Somali Current, *J. Phys. Oceanogr.*, *12*, 1325–1342, 1982.

Legler, D. M., I. M. Navon, and J. J. O'Brien, Objective analysis of pseudo-stress over the Indian Ocean using a direct-minimization approach, *Mon. Weather Rev.*, in press, 1988.

Lighthill, M. J., Dynamic response of the Indian Ocean to onset of the southwest monsoon, *Philos. Trans. R. Soc. London, Ser. A*, *265*, 45–92, 1969.

Lin, L. B., and H. E. Hurlburt, Maximum simplification of nonlinear Somali Current dynamics, in *Monsoon Dynamics*, edited by M. J. Lighthill and R. P. Pearce, pp. 541–555, Cambridge University Press, New York, 1981.

Luther, M. E., and J. J. O'Brien, A model of the seasonal circulation in the Arabian Sea forced by observed winds, *Prog. Oceanogr.*, *14*, 353–385, 1985.

Luther, M. E., J. J. O'Brien, and A. H. Meng, Morphology of the Somali Current system during the southwest monsoon, in *Coupled Ocean-Atmosphere Models*, edited by J. C. J. Nihoul, pp. 405–437, Elsevier Amsterdam, 405–437, 1985.

Navon, I. M., and D. M. Legler, Conjugate-gradient methods for large scale minimization in meteorology, *Mon. Weather Rev.*, *115*, 1479–1505, 1987.

Schott, F., Monsoon response of the Somali Current and associated upwelling, *Prog. Oceanogr.*, *12*, 357–382, 1983.

Schott, F., and D. R. Quadfasel, Variability of the Somali Current system during the onset of the southwest monsoon, *J. Phys. Oceanogr.*, *12*, 1343–1357, 1982.

Swallow, J. C., and M. Fieux, Historical evidence for two gyres in the Somali Current, *J. Mar. Res.*, *40*, suppl., 747–755, 1982.

Swallow, J. C., R. L. Molinari, J. G. Bruce, O. B. Brown, and R. H. Evans, Development of near-surface flow pattern and water mass distribution in the Somali Basin, in response to the southwest monsoon in 1979, *J. Phys. Oceanogr.*, *13*, 1398–1415, 1983.

D. M. Legler, M. E. Luther, and J. J. O'Brien, Mesoscale Air-Sea Interaction Group, Florida State University, Tallahassee, FL 32306.

R. C. Simmons, NAVWEST Ocean Center, Box 113, Pearl Harbor, HI 96860.

(Received October 5, 1987;
revised July 24, 1988;
accepted August 11, 1988.)

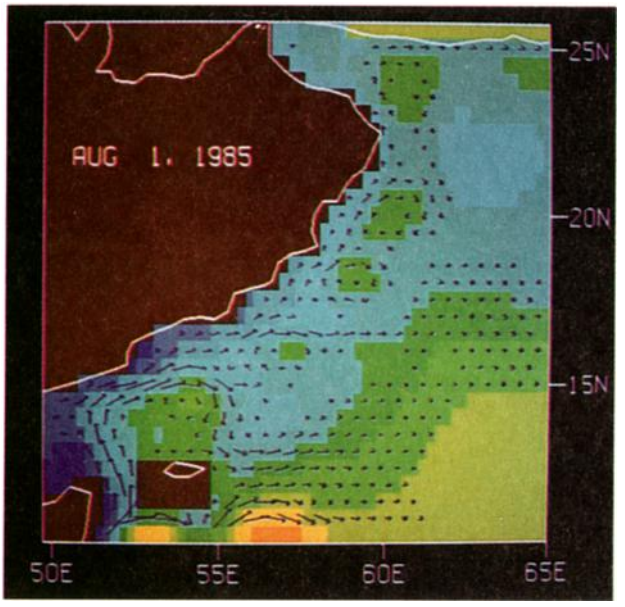

Plate 1*a*

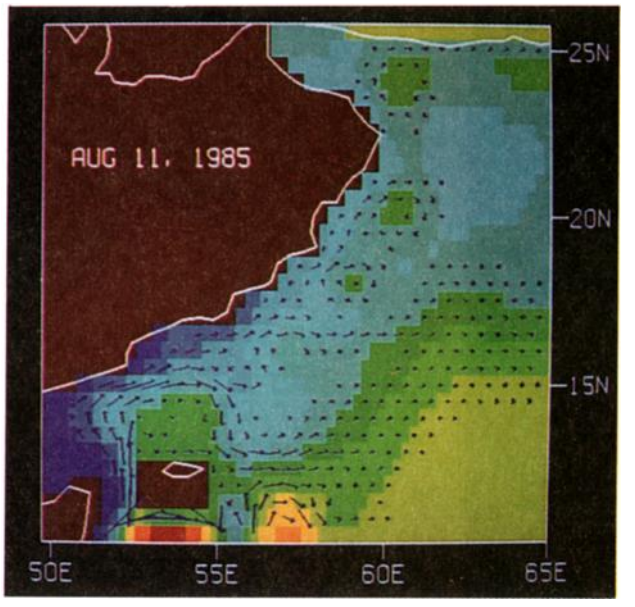

Plate 1*b*

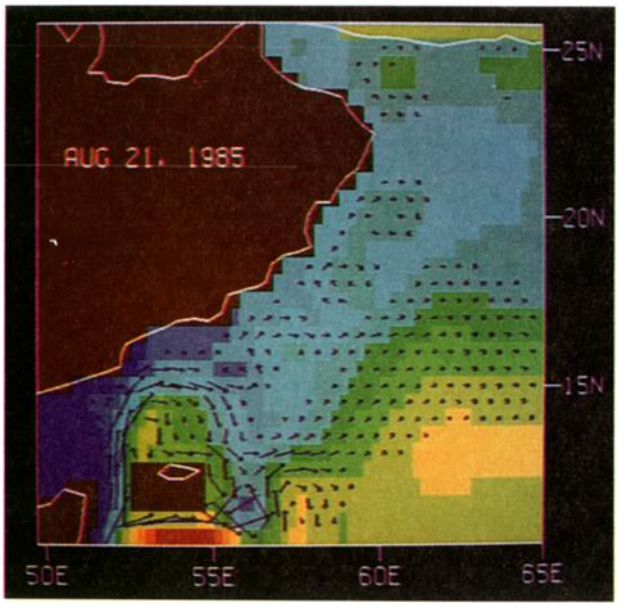

Plate 1*c*

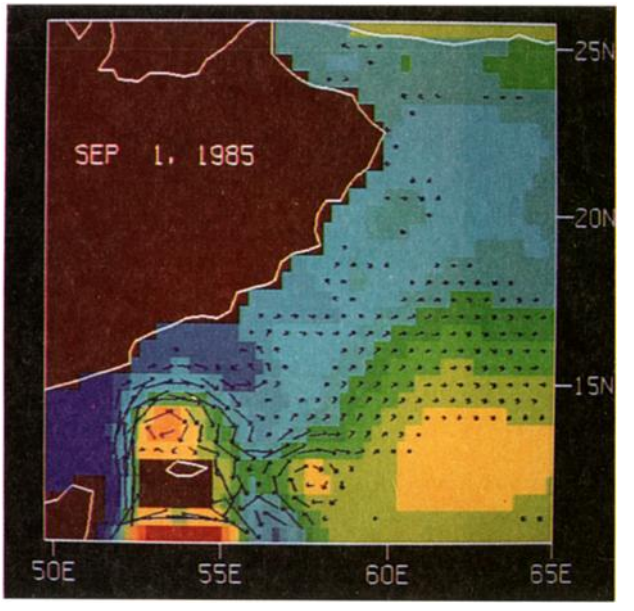

Plate 1*d*

Plate 1 [*Simmons et al.*]. Formation of the eddies around Socotra. Model fields are shown every 10 days from August through October for the northwestern corner of the model basin. Arrows show upper layer velocity, with only two arrows shown per degree in both directions. Velocities of less than 0.05 m/s are suppressed, and velocities larger than 0.8 m/s are truncated to 0.8 m/s for clarity. Color indictes upper layer thickness, with blue shades indicating thinner (cooler) upper layer and red to yellow shades indicating thicker (warmer) upper layer. Dark blue indicates values of 140 m, medium green indicates values of 190–200 m, and dark red indicates values of 240 m, with color gradations at 10-m intervals. The great whirl forms to the south of this region in late June under the direct influence of the Findlater Jet and moves northward in late July until it impinges on the south coast of Socotra. Some outflow from the great whirl passes through the channel between Socotra and Ras Asir, while additional outflow continues eastward and meanders into the interior (Plates 1*a*–1*c*). The North Socotra Warm and Cold eddies form in early September in the meandering outflow from the channel west of Socotra (Plates 1*d*–1*f*). The Socotra Eddy initially forms in the outflow east of the great whirl (Plate 1*a*) and then moves northward and intensifies as it merges with an area of high ULT that propagates westward from the interior as a Rossby wave (Plates 1*c*–1*f*). A tongue of low ULT separates the Socotra Eddy from the coast. This cold tongue forms to the northeast of the great whirl (Plate 1*b*) and is advected around the great whirl to the southeast.

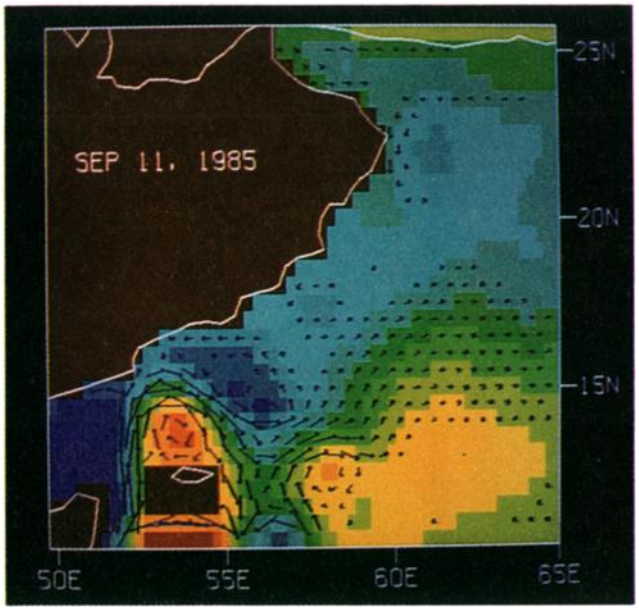

Plate 1*e*

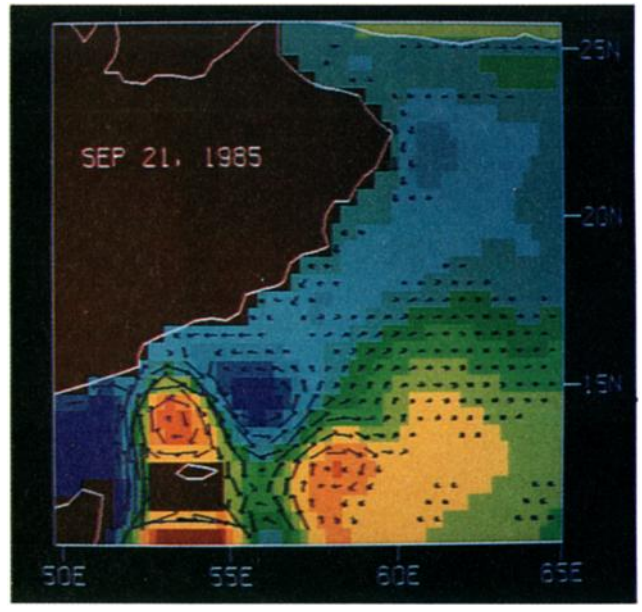

Plate 1*f*

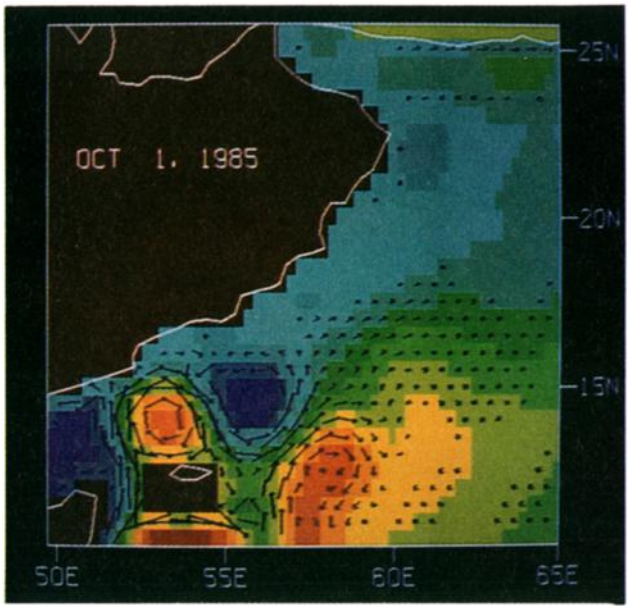

Plate 1*g*

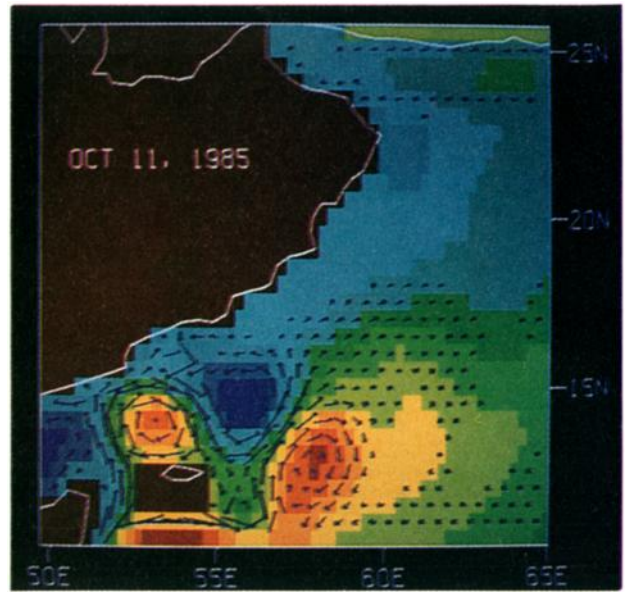

Plate 1*h*

Plate 1 [*Simmons et al.*]. (continued)

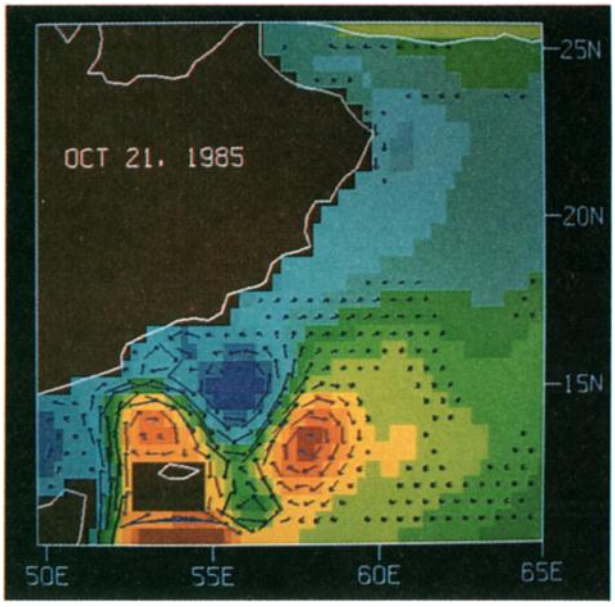

Plate 1*i*

Plate 1 [*Simmons et al.*]. (continued)

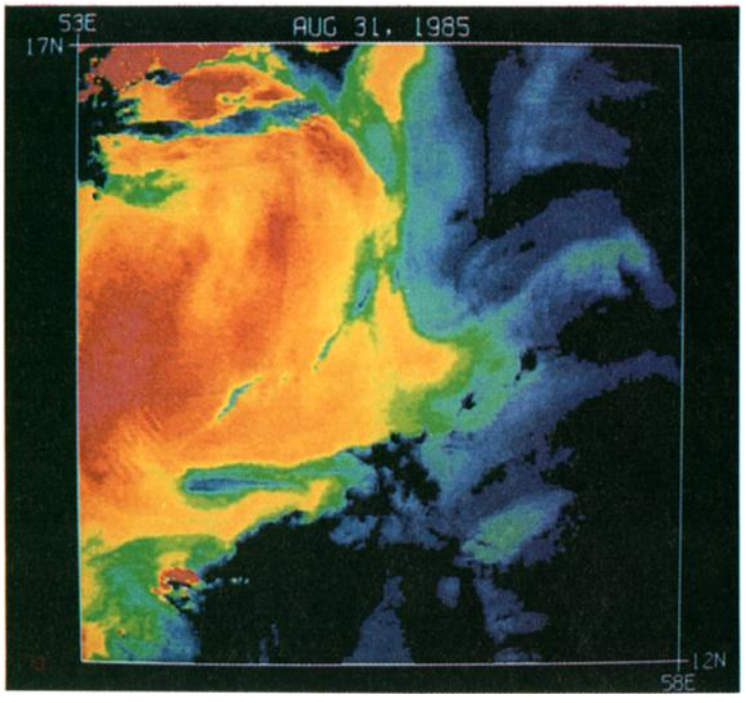

Plate 2 [*Simmons et al.*]. The NOAA 8 AVHRR image of August 30, 1985, for the region south of the Yemen coast. The blue region along the eastern half of the image indicates cooler sea surface temperatures, indicative of the North Socotra Cold Eddy, while the yellow and red region to the west indicates warm surface temperatures, indicative of the North Socotra Warm Eddy. Black indicates missing data. Socotra is in the lower left corner of the image.